Forschungszentrum Karlsruhe

Technik und Umwelt

Wissenschaftliche Berichte

FZKA 6211

A Model for PZT Ceramics under Uni-Axial Loading

M. Kamlah, Q. Jiang*

Institut für Materialforschung

*University of California, Riverside, College of Engineering, USA

Forschungszentrum Karlsruhe GmbH, Karlsruhe

1998

Abstract

Our aim is the motivation of a macroscopic constitutive model for engineering reliability analysis purposes of piezoceramic components designed for so-called "smart" electromechanical sensor and actuator applications. Typically, such components are made of materials like ferroelectric PZT ceramics which exhibit significant history dependent nonlinearities as the well known dielectric, butterfly, and ferroelastic hystereses due to switching processes. Furthermore, phase transitions lead to distinct thermo-electromechanical coupling properties and rate effects are present.

In a first step, we propose a constitutive framework capable of representing general thermo-electromechanical processes. This framework makes use of internal variables and is thermodynamically consistent with the Clausius-Duhem inequality for all admissible processes.

Next, we focus on uni-axial electromechanical loadings and introduce microscopically motivated internal variables and their evolution equations. In order to verify the underlying a priori assumptions, we discuss extensively the numerically calculted model response to standard electromechanical loading paths. It turns out that the model represents the typical hystereses mentioned above as well as mechanical depolarization and other nonlinear electromechanical coupling phenomena. Furthermore, the model response exhibits rate effects.

Ein Modell für PZT-Keramiken unter einachsigen Belastungen

Unser Ziel ist die Motivation eines makroskopischen Stoffgesetzes zum Zwecke strukturmechanischer Zuverlässigkeitsanalysen von piezokeramischen Komponenten für sogenannte "intelligente" elektromechanische Sensor- und Aktuatoranwendungen. Meist werden solche Komponenten aus ferroelektrischen PZT-Keramiken hergestellt, die infolge von Umklappprozessen ausgeprägt geschichtsabhängige Nichtlinearitäten aufweisen wie die wohlbekannte dielektrische Hysterese, die Schmetterlingshysterese und die ferroeleastische Hysterese. Auch führen Phasenübergänge zu bestimmten thermo-elektromechanischen Koppelphänomenen, und es treten Geschwindigkeitseffekte auf.

In einem ersten Schritt schlagen wir einen Modellrahmen vor, der geeignet ist, allgemeine thermo-elektromechanische Prozesse zu erfassen. Dieser Modellrahmen beruht auf inneren Variablen und ist thermodynamisch konsistent für alle zulässigen Prozesse.

Als nächstes beschränken wir uns auf einachsige elektromechanische Belastungen und führen mikroskopisch motivierte innere Variable mit ihren Evolutionsgleichungen ein. Um unsere A-Priori-Annahmen zu verifizieren, diskutieren wir ausführlich die numerisch berechnete Antwort auf übliche elektromechanische Belastungspfade. Es zeigt sich, daß das Modell die oben erwähnten typischen Hysteresen, sowie auch die mechanische Depolarisation und andere nichtlineare elektromechanische Koppelphänomene darstellt. Weiterhin zeigt das Modell Geschwindigkeitseffekte.

Contents

1 Introduction

The piezoelectric effect causes a coupling between electric and mechanical fields, and thus it is a number one candidate for advanced sensor and actuator applications (e. g. [1]). In many cases, the piezoelectric effect is realized by the ferroelectric phase of lead zirconate titanate (PZT) ceramics [2, 3, 4]. If such a material has been poled by an electric field above the coercitive field at a temperature below the Curie point, its response to small signals may be characterized by the parameters of classical linear piezoelectricity. However, nowadays applications involve severe loadings and complicated geometries such that the assumption of small signals is no longer justified in general. Rather, the nonlinear behavior of the material can become dominant [5], and it may have an impact on its fatigue properties [6, 7].

In order to assess the reliability of a piezoceramic component, it is important for structural engineers to estimate its mechanical stress state quantitatively. For this purpose, the electric and mechanical field equations have to be solved for an appropriate constitutive assumption relating the histories of the macroscopic stresses, strains, electric field, and polarization to each other.

The constitutive theory of linear piezoelectricity was developed many decades ago and has found wide spread application in analytical and numerical solution methods (cf. [8, 9, 10]). Many recent works deal with linear piezoelectric fracture mechanics, see [11, 12, 13, 14, 15, 16, 17]. We may emphasize that in principle the significance of results based on linear piezoelectricity is restricted to cases where the assumption of linear behavior is met with sufficient accuracy.

Works dealing with nonlinear constitutive models of piezoceramics for purposes of engineering reliabilty analyses are still quite rare. A pure phenomenological approach for the experimental investigation and description of constitutive behavior has been invented in [18, 19, 20, 21, 22]. An attempt to describe macroscopic ferroelectricity on a thermodynamical basis can be found in [23, 24]. [25, 26, 27] are important experimental works investigating nonlinear electromechanical coupling phenomena. The papers [28, 29, 30, 31] present two successful attempts to describe electrostrictive coupling by means of thermodynamically based phenomenological models.

In [32], a phenomenological constitutive model of PZT ceramics for general electromechanical loading histories has been proposed, which is simple enough to be implemented in a FE-code with reasonable expenditure. Remanent polarization and remanent strain have been introduced as internal variables and by bilinear approximation the macroscopic electromechnical coupling phenomena relevant for engineering applications of these materials are represented. The model has been motivated directly from exerimental findings without reference to a thermodynamical framework. It shows no time effects, since the evolutions equations of the internal variables are rate independent.

Some recent approaches simulate macroscopic ferroelectricity on the basis of microscopic models for the behavior of single domains. In [33], a model consisting of 10 000 randomly oriented grains, has been simulated numerically, where each grain shows an idealized rectangular hysteresis for the dielectric behavior. With the help of an energet-

ically motivated criterion for domain switching caused by an electric field or mechanical stress, the macroscopic dielectric and butterfly hystereses are described. Following a similar approach, the model in [34] utilizes the additional constraint that each single grain is transversly isotropic (instead of possesing tetragonal anisotropy) and as a consequence, macroscopic constitutive behavior is derived analytically from microscopic assumptions.

One of the primary difficulties in modeling of macroscopic behavior of ferroelectric ceramics associated with domain switching is the drastic difference of the length scale of ferroelectric domains from that of macroscopic specimens. To overcome this difficulty, some investigators [33, 35] have proposed to treat each grain as a single effective domain. This approach is computationally effective and hence permits simulations of specimens consisting of a large number of grains, although it has several shortcomings, such as lack of a mechanism to determine the magnitude of the effective polarisation intensity. In [36], it recently has been proposed to model each grain as a body of mixture consisting of distinct types of domains which are characterized by their mass fraction as internal variables. The average polarization of a grain is hence a linear function of the mass fractions and domain switching corresponds to changes of the mass fractions of the corresponding domains. The numerical implementation of this model has been limited to either one dimensional cases [37] or two-dimensional cases with a few hundreds of grains [38] because of the complexity of the formulation.

The scope of this paper is to present an approach towards a macroscopic constitutive model for ferroelectric ceramics applicable by structural engineers to reliability analyses which is microscopically motivated and thermodynamically based at the same time.

In section 2, we invent the general structure of our model. A thermodynamic Gibbs energy function is constructed such that classical linear piezoelectricity is included as a special case. It has to be taken into account that the anisotropy properties of the classical electromechanical tensors as well as macroscopic remanent polarization and strain depend on the loading history. This is done by introducing so-called microstructural parameters as internal variables which are supposed to represent the state of the microdipoles in the ceramic in a macroscopic manner. The Clausius-Duhem inequality can be fulfilled in sufficient manner for every admissible electromechanical process, if the evolution equations for the internal variables are given a special structure.

In the literature, experimental data for nonlinear coupling phenomena of piezoceramics are available only for uni-axial electromechanical loadings. Therefore, we specialize our considerations to this case in section 3. As a main step, two internal variables are motivated representing the macroscopic state of the orientation of the crystal axes and of the spontaneous polarization, respectively, of the unit cells in the polycrystal. The evoltion equations of these internal variables are introduced such that the model response shows nonlinear rate effects. A threshold takes care that only external loads of sufficient magnitude can lead to an evolution of the microstructural parameters, i. e. to an onset of ferroelectric switching processes.

The system of constitutive equations is too complicated to be investigated analytically. In order to verify the physical significance of the model, we discuss in sections 4 and 5 by means of numerical integration the model response to standard electromechanical loading

histories. Special emphasis is layed on the microscopic interpretation of the behavior of the macroscopic quantities.

In the following analysis which is restricted to a geometrically linear setting, all component representations of tensors are refered to a cartesian coordinate system (summation convention). First order tensors (*vectors*) are denoted by upright letters with superscript arrows ($\vec{\mathrm{a}}$, $\vec{\mathrm{A}}$) and second order tensors (*tensors*) by bold slanted letters ($\boldsymbol{a}$, $\boldsymbol{A}$, $\boldsymbol{\alpha}$). A dot between tensors indicates the contraction relative to one index, for example, the inner product between vectors, i. e. $\vec{\mathrm{a}} \cdot \vec{\mathrm{b}} = \mathrm{a}_i \mathrm{b}_i$, the composition of two tensors, i. e. $\boldsymbol{A} \cdot \boldsymbol{A}^{-1} = \boldsymbol{I}$ ($\boldsymbol{A}^{-1}$: inverse of $\boldsymbol{A}$, $\boldsymbol{I}$: identity tensor), the inner product between tensors, i. e. $\boldsymbol{A} : \boldsymbol{B} = \mathrm{tr}(\boldsymbol{A} \cdot \boldsymbol{B}^T) = A_{ij} B_{ij}$ (tr$\boldsymbol{A}$: trace of $\boldsymbol{A}$. $\boldsymbol{B}^T$: transpose of $\boldsymbol{B}$), $\dot{()} = \mathrm{d}()/\mathrm{d}t$ denotes the time derivative of a field ().

2 Thermodynamical Framework

By definition, a ferroelectric material exhibits polarization switching at attainable electric fields [39]. As a result, the well known ferroelectric hysteresis occurs for loadings by a cyclic electric field. Switching processes can also be initiated by mechanical loadings leading to ferroelastic behavior (e. g. [26]). On the macroscopic level, these hysteresis phenomena represent irreversible changes in the material and they can be observed for arbitrary slow loadings [18].

The above findings motivated us to decompose strain and polarization additively in reverible and irreversible parts (see also [23, 24]):

$$\boldsymbol{S} = \boldsymbol{S}^{\mathrm{r}} + \boldsymbol{S}^{\mathrm{i}} \tag{1}$$

$$\vec{\mathrm{P}} = \vec{\mathrm{P}}^{\mathrm{r}} + \vec{\mathrm{P}}^{\mathrm{i}} \tag{2}$$

The *irreversible* or *remanent* quantities $\boldsymbol{S}^{\mathrm{i}}$ and $\vec{\mathrm{P}}^{\mathrm{i}}$ represent macroscopic averages of the microscopic spontaneous strain and polarization of the ferroelectric crystal structure, respectively. In order to represent the history dependence of irreversible strain and polarization, we consider them to be functions of a set of internal variables:

$$\boldsymbol{S}^{\mathrm{i}} = \hat{\boldsymbol{S}}^{\mathrm{i}} (q_1, \ldots, q_n) \tag{3}$$

$$\vec{\mathrm{P}}^{\mathrm{i}} = \hat{\vec{\mathrm{P}}}^{\mathrm{i}} (q_1, \ldots, q_n) \tag{4}$$

The association of the internal variables $q_1, \ldots, q_n$ with microstructural parameters should be introduced such that they reflect on the macroscopic level the internal microscopic state of the material.

Besides the above mentioned microstrucutural changes, ferroelectic ceramics may respond to electro-mechanical loadings without changes of the lattice structure. We represent this reversible piezoelectric behavior by the *reversible* quantities $\boldsymbol{S}^{\mathrm{r}}$ and $\vec{\mathrm{P}}^{\mathrm{r}}$. For a fixed internal state, the piezoelectric properties of the material can be approximated by linear relations. In this sense, it seems apropriate to choose the relations

$$\boldsymbol{S}^{\mathrm{r}} = \mathbb{C}^{-1} : \boldsymbol{T} + \mathbf{dl}^T \cdot \vec{\mathrm{E}} \tag{5}$$

$$\vec{\mathrm{P}}^{\mathrm{r}} = \mathbf{dl} : \boldsymbol{T} + \boldsymbol{\epsilon} \cdot \vec{\mathrm{E}} \tag{6}$$

for the reversible strain and polarization where $\boldsymbol{T}$ is the *stress* and $\vec{\mathrm{E}}$ is the *electric field*. Although these equations have the same stucture as the classical linear piezoelectric constitutive law, the *elasticity tensor* $\mathbb{C}$, the *tensor of piezoelectric constants* $\mathbf{dl}$, and the *tensor of dielectric constants* $\boldsymbol{\epsilon}$ depend on the loading history via the internal variables:

$$\mathbb{C} = \hat{\mathbb{C}}\ (q_1, \ldots, q_n) \tag{7}$$

$$\mathbf{dl} = \hat{\mathbf{dl}}\ (q_1, \ldots, q_n) \tag{8}$$

$$\boldsymbol{\epsilon} = \hat{\boldsymbol{\epsilon}}\ (q_1, \ldots, q_n) \tag{9}$$

In this way we take into account the sensitivity of the reversible properties of the ceramic to changes in the lattice structure. In particular, the history dependence of these tensors is related to history dependent anisotropy properties. This may be most pronounced in the case of $\mathbf{dl}$, since the phenomenon of piezoelectrical coupling is absent on the macroscopic level in an unpoled material even if its microstructure exhibits a microscopic spontaneous polarization.

Until now, we have motivated a certain model structure for the description of the electro-mechanical behavior of ferroelectric ceramics in a first step. In the next step, we want to find a thermodynamical basis for this model structure. For this purpose, we depart from the Clausius-Duhem inequality for a deformable dielectric body which reads in an isothermal process with uniform temperature distribution as

$$\boldsymbol{T} : \dot{\boldsymbol{S}} + \vec{\mathrm{E}} \cdot \dot{\vec{\mathrm{P}}} \geq \rho\, \dot{\psi} \tag{10}$$

where ρ is the *mass density*. The *free energy* ψ has to be constructed such that it is compatible with the piezelectricity relations (5) and (6) in view of the inequality (10). The free energy should depend on both the reversible quantities $\boldsymbol{S}^{\mathrm{r}}$, $\vec{\mathrm{P}}^{\mathrm{r}}$ and the remanent quantities $\boldsymbol{S}^{\mathrm{i}}$, $\vec{\mathrm{P}}^{\mathrm{i}}$. Noting the relations in (1) and (2), we write

$$\psi = \bar{\psi}(\boldsymbol{S}^{\mathrm{r}}, \vec{\mathrm{P}}^{\mathrm{r}}, q_1, \ldots, q_n) \tag{11}$$

Then, we find the potential relations

$$\boldsymbol{T} = \rho\, \frac{\partial \bar{\psi}}{\partial \boldsymbol{S}^{\mathrm{r}}}(\boldsymbol{S}^{\mathrm{r}}, \vec{\mathrm{P}}^{\mathrm{r}}, q_1, \ldots, q_n) \tag{12}$$

$$\vec{\mathrm{E}} = \rho\, \frac{\partial \bar{\psi}}{\partial \vec{\mathrm{P}}^{\mathrm{r}}}\,(\boldsymbol{S}^{\mathrm{r}}, \vec{\mathrm{P}}^{\mathrm{r}}, q_1, \ldots, q_n) \tag{13}$$

as necessary and sufficient conditions for the Clausius-Duhem inequality (10) to be satisfied for reversible processes in the sense $\dot{q}_\alpha = 0\ ,\ \alpha = 1, \ldots, n$.

Assuming the relations (12) and (13) can be solved for $\boldsymbol{S}^{\mathrm{r}}$, $\vec{\mathrm{P}}^{\mathrm{r}}$, we may introduce by the Legendre transform

$$\rho\, g = -\rho\, \psi + \boldsymbol{T} : \boldsymbol{S}^{\mathrm{r}} + \vec{\mathrm{E}} \cdot \vec{\mathrm{P}}^{\mathrm{r}} \tag{14}$$

the *Gibbs engergy*

$$g = \tilde{g}(\boldsymbol{T}, \vec{\mathrm{E}}, q_1, \ldots, q_n) \quad . \tag{15}$$

Using (12) and (13), we obtain

$$\boldsymbol{S}^{\mathrm{r}} = \rho \frac{\partial \tilde{g}}{\partial \boldsymbol{T}}(\boldsymbol{T}, \vec{\mathrm{E}}, q_1, \ldots, q_n) \tag{16}$$

$$\vec{\mathrm{P}}^{\mathrm{r}} = \rho \frac{\partial \tilde{g}}{\partial \vec{\mathrm{E}}}(\boldsymbol{T}, \vec{\mathrm{E}}, q_1, \ldots, q_n) \quad . \tag{17}$$

For fixed $q_1, \ldots, q_n$, (16) and (17) represent the piezoelectric behavior which we assume to be linear in (5) and (6). Consequently, the dependence of

$$g = \tilde{g}^{\mathrm{r}}(\boldsymbol{T}, \vec{\mathrm{E}}, q_1, \ldots, q_n) + \tilde{g}^{\mathrm{i}}(q_1, \ldots, q_n) \tag{18}$$

upon $\boldsymbol{T}$ and $\vec{\mathrm{E}}$ is quadratic, i e.,

$$\rho\, g^{\mathrm{r}} = \frac{1}{2}\, \boldsymbol{T} : \hat{\boldsymbol{\mathcal{C}}}^{-1} : \boldsymbol{T} \; + \; \vec{\mathrm{E}} \cdot \hat{\mathbf{dl}} : \boldsymbol{T} \; + \; \frac{1}{2}\, \vec{\mathrm{E}} \cdot \hat{\boldsymbol{\epsilon}} \cdot \vec{\mathrm{E}} \quad , \tag{19}$$

which posseses the formal structure of classical linear piezoelectricity. In fact, by the potential properties (16) and (17) we find the piezoelectric relations (5) and (6). However, in contrast to linear piezoelectricity the coefficients $\boldsymbol{\mathcal{C}}$, $\mathbf{dl}$, and $\boldsymbol{\epsilon}$ are functions of the internal variables $q_1, \ldots, q_n$. Thus, we now may determine the free energy function $\bar{\psi}$ by the Legendre transform (14) which is consistent with the basic properties (1) through (9) in the sense of the Clausius-Duhem inequality.

Next, we want to exploit the Clausius-Duhem inequality in view of restrictions for the evolution equations of the internal variables. With the help of the potential relations (16) and (17), we find from the Legendre transform (14)

$$\rho\, \dot{\psi} = \boldsymbol{T} : \dot{\boldsymbol{S}}^{\mathrm{r}} + \vec{\mathrm{E}} \cdot \dot{\vec{\mathrm{P}}}^{\mathrm{r}} - \rho \sum_{\alpha=1}^{n} \frac{\partial \tilde{g}}{\partial q_\alpha}\, \dot{q}_\alpha \quad . \tag{20}$$

Inserting this in inequality (10) and taking into account the additive decompositions (1) and (2) of $\boldsymbol{S}^{\mathrm{i}}$ and $\vec{\mathrm{P}}^{\mathrm{i}}$ as well as their dependences (3) and (4) on the internal variables yields

$$\sum_{\alpha=1}^{n} \left(\boldsymbol{T} : \frac{\partial \hat{\boldsymbol{S}}^{\mathrm{i}}}{\partial q_\alpha} \; + \; \vec{\mathrm{E}} \cdot \frac{\partial \hat{\vec{\mathrm{P}}}^{\mathrm{i}}}{\partial q_\alpha} \; + \; \frac{\partial \tilde{g}}{\partial q_\alpha} \right) \dot{q}_\alpha \; \geq \; 0 \quad . \tag{21}$$

Following [36, 37], we call motivated by this inequality the quantities

$$f_\alpha = \boldsymbol{T} : \frac{\partial \hat{\boldsymbol{S}}^{\mathrm{i}}}{\partial q_\alpha} \; + \; \vec{\mathrm{E}} \cdot \frac{\partial \hat{\vec{\mathrm{P}}}^{\mathrm{i}}}{\partial q_\alpha} \; + \; \frac{\partial \tilde{g}}{\partial q_\alpha} \quad , \quad \alpha = 1, \ldots, n \tag{22}$$

driving forces. The remaining inequality (21) and thus the Clausius-Duhem inequality is satisfied in a sufficient manner, if we assume

$$\dot{q}_\alpha = \Lambda_\alpha f_\alpha \quad , \quad \Lambda_\alpha \geq 0 \quad , \quad \alpha = 1, \ldots, n \quad . \tag{23}$$

3 Microscopically motivated internal variables for uni-axial loadings

We now specialize the general frame work introduced in the previous section to the case of uni-axial electro-mechanical loadings of a ferroelectric ceramic. The properties of the ferroelectric phase of the polycrystal are assumed to be dominated by the tetragonality of the microstructure. Consideration of a tetragonal microstructure offers probably the most obvious insight in the relation between microstructure and macroscopic response.

A tetragonal unit cell is characterized by the fact that one of its lattice axes, the so-called c axis is about 0.1 % longer than the two other ones, the a axes. The c axes of the unit cells can be oriented in either one of the three lattice directions of a grain. A region within a grain of the ferroelectric polycrystal where the c axes of the unit cells have the same orientation is called a *domain*. It is a characteristic property of ferroelectric materials that mechanical or electrical loadings may switch the orientation of the c axes by 90° and 180°.

In the thermally depoled *reference state* of the polycrystalline ceramic, the ditribution of the c axes is random and no direction is preferred. In case of uni-axial loadings, the axis of the loading may eventually become preferred such that the ceramic will exhibit transvesal isotropy on the macroscopic level irrespective of the details of its microstructural anisotropy properties. While the axis of anisotropy will be fixed to coincide with direction of the loading, the extend of anisotropy may vary with the loading history.

3.1 Uni-axial formulation of the model

The direction of the uni-axial loading is assumed to coincide with the x_3 axis. We denote the only non-vanishing components of $\boldsymbol{T}$, $\vec{\mathrm{E}}$, $\vec{\mathrm{P}}$, and $\vec{\mathrm{P}}^{\mathrm{i}}$ by σ, E, P, and P^{i}, respectively. Furthermore, we write $S = S_{33}$ and $S^{\mathrm{i}} = S^{\mathrm{i}}_{33}$ for the relevant components of the strain tensors $\boldsymbol{S}$ and $\boldsymbol{S}^{\mathrm{i}}$, respectively.

The additive decompositions (1) and (2) then read as

$$S = S^{\mathrm{r}} + S^{\mathrm{i}} \tag{24}$$

$$\mathrm{P} = \mathrm{P}^{\mathrm{r}} + \mathrm{P}^{\mathrm{i}} \quad . \tag{25}$$

From the piezoelectricity relations (5) and (6) we may write

$$S^{\mathrm{r}} = \frac{1}{\hat{Y}}\,\sigma + \hat{\mathrm{d}}\,\mathrm{E} \tag{26}$$

$$\mathrm{P}^{\mathrm{r}} = \hat{\mathrm{d}}\,\sigma + \hat{\epsilon}\,\mathrm{E} \tag{27}$$

where $\hat{Y} = 1/(\hat{\boldsymbol{\mathcal{C}}}^{-1})_{3333}$, $\hat{\mathrm{d}} = (\hat{\mathbf{dl}})_{333}$, and $\hat{\epsilon} = \hat{\epsilon}_{33}$ are functions of the microstructural parameters q_α. Additionally, we find

$$\rho\, g^{\mathrm{r}} = \frac{1}{2}\,\frac{1}{\hat{Y}}\,\sigma^2 + \hat{\mathrm{d}}\,\sigma\,\mathrm{E} + \frac{1}{2}\,\hat{\epsilon}\,\mathrm{E}^2 \tag{28}$$

with these definitions.

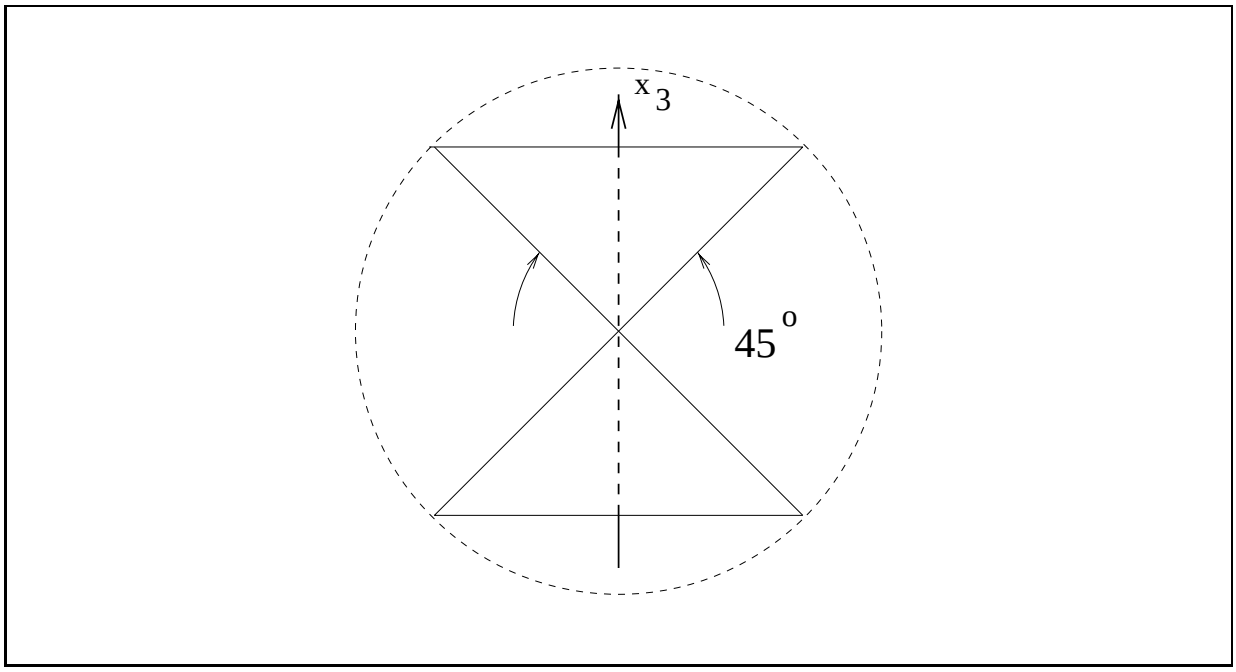

Fig. 1: Two cones of 45° about the x_3 axis, being the axis of loading: The value of β is the fraction of c axes situated with in these cones.

3.2 Choice of microstructural parameters

The physical significance of model depends strongly on the choice of the internal variables q_α. For the considered case of uni-axial loadings, we will now introduce such microstructural parameters. They represent the microscopic state of the ceramic in the sense of macroscopic averages.

To begin with, we consider a ferroelectric sample in its unpoled reference state. It is well known that such a sample exhibits irreversible deformation under compressive stresses of sufficient magnitude without any changes of the state of macroscopic polarization [25, 26]. This phenomenon stems from so-called 90° switching processes of the c axes of the tetragonal unit cells. While the distribution of the c axes was initially uniform over the spherical surface, the fraction of c axes aligned with the x_3 axis, the axis of loading, is reduced due to 90° switching processes. The the length of the sample in the direction of loading is decreased irreversibly and it gives way for the compressive stress.

We now introduce cones of 45° angle with the x_3 axis being the cone axis, see Fig. 1. Obviously, the fraction of of domains with their c axis situated within these cones has been reduced in the previously discussed example of mechanical compressive loadings. Thus the microscopic state of the distribution of the c axes may be described with the help of thess cones: Our first internal variable, denoted by $\beta = q_1$, represents the fraction of domains with their c axes situated within the 45° cones. This means that β may take values between 0 and 1. From the above discussion we see that the irrevesible deformation S^{i} should be chosen as a function of β.

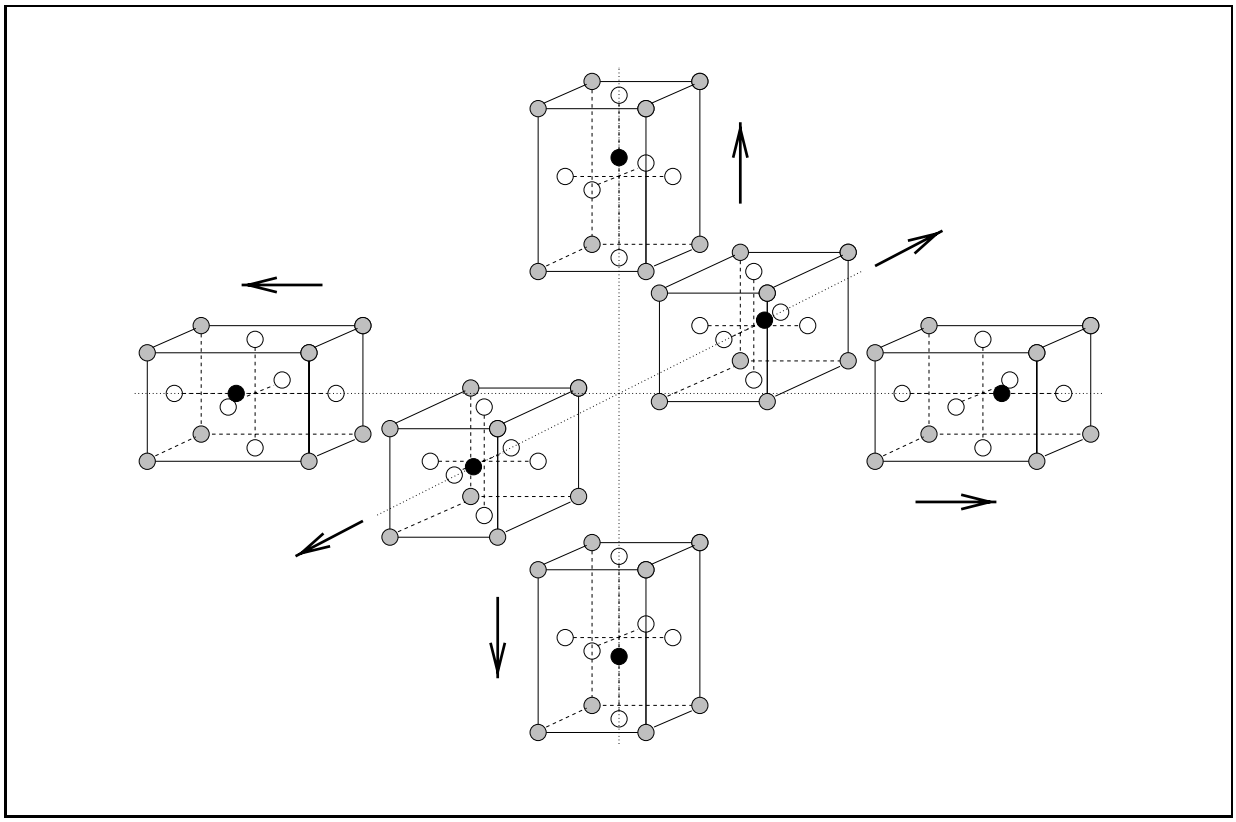

Fig. 2: Within the lattice of a tetragonal grain, there are six possible orientations for the microdipole of the polarized unit cell (two per lattice axis).

The tetragonal unit cell of a ferroelectric material is polarized: The resultant centers of positive and negative charges constituting the unit cell have different locations. Thus every unit cell forms a microdipole with its axis parallel to the c axis of the unit cell. Within a grain, there are six possible orientations for the microdipole of a unit cell. In particular, there are two orientations for each lattice direction (see Fig. 2). Concerning the net polarization resulting from the microdipoles this means that different states of macroscopic polarization can result from the same degree of alignment of the c axes with respect to the x_3 axis, i. e., for the same value of β. Therefore, we need additional information, in order to determine the macroscopic state of polarization associated with the microscopic domain state.

In this sense, our second internal variable $\gamma = q_2$ represents the state of relative net polarization in x_3 direction resulting from the distribution of the spontaneous microdipoles:

$$\gamma = \frac{P^i}{P_{sat}} \tag{29}$$

In this equation, the *saturation polarization* P_{sat} is the maximum macroscopic irreversible polarization.

3.3 Relations between irreversible quantities and microstructural parameters

We now want to specify the dependence of irreversible strain on the microstructural parameters. As mentioned before, the macroscopic state of irreversible strain depends on β, the fraction of domains with their c axes aligned to the x_3 axis. However, the state of relative polarization of these domains will have no influence on the remanent distortion of the lattice. Thus we may assume

$$S^{\mathrm{i}} = \hat{S}^{\mathrm{i}}(\beta) \tag{30}$$

for the functional relation between the macroscopic irreversible strain and the microstructural state variables. For convenience, we may identify the unpoled reference state with a vanishing value of the irreversible strain: $\hat{S}^{\mathrm{i}}(\beta_{\mathrm{ref}}) = 0$. If all c axes are situated in the 45° cones about the x_3 axis, i.e. $\beta = 1$, the irreversible strain reaches a saturation value: $\hat{S}^{\mathrm{i}}(1) = S_{\mathrm{sat}}$. Here, the *saturation strain* S_{sat} is the maximum value of the macroscopic remanent strain of the ceramic which is assumed for a domain state of highest order with respect to a certain axis. By resticting ourselves to a linear relation for the sake of simplicity, we find the relation

$$\hat{S}^{\mathrm{i}}(\beta) \;=\; S_{\mathrm{sat}}\,\frac{\beta - \beta_{\mathrm{ref}}}{1 - \beta_{\mathrm{ref}}} \tag{31}$$

from the two values just discussed.

As a verification, it is interesting to consider the state $\beta = 0$ where all c axes are situated outside of the 45° cones. Such a state might be reached by strong compressive stresses acting in x_3 direction. In this case, we find $\hat{S}^{\mathrm{i}}(0) = -S_{\mathrm{sat}}\,\beta_{\mathrm{ref}}/(1-\beta_{\mathrm{ref}})$. However, in order to be able discuss this value, we must specify β_{ref}. Since β_{ref} represents the the thermally depoled reference state, its value is given by the intersection of our 45° cones with the spherical surface or in other words by the cutoff of the spherical surface by these cones. This value is slightly below one third, so that we may assume

$$\beta_{\mathrm{ref}} = \frac{1}{3} \tag{32}$$

for simplicity. We then get $\hat{S}^{\mathrm{i}}(0) = -\frac{1}{2}S_{\mathrm{sat}}$. In a ferroelectric material with a tetragonal microstructure one may expect such a difference in the maximum magnitudes of the irreversible strain for compressive and tensile loadings at least qualitatively (see also section 4.2 of this paper and [40] for experimental evidence on this matter).

For the sake of completeness, we may note at this point that we find from the defintion (29) of the second internal variable γ immediately

$$\mathrm{P}^{\mathrm{i}} = \gamma\,\mathrm{P}_{\mathrm{sat}} \tag{33}$$

This means that the irreversible polarization depends on the relative polarization γ alone: $\mathrm{P}^{\mathrm{i}} = \hat{\mathrm{P}}^{\mathrm{i}}(\gamma)$

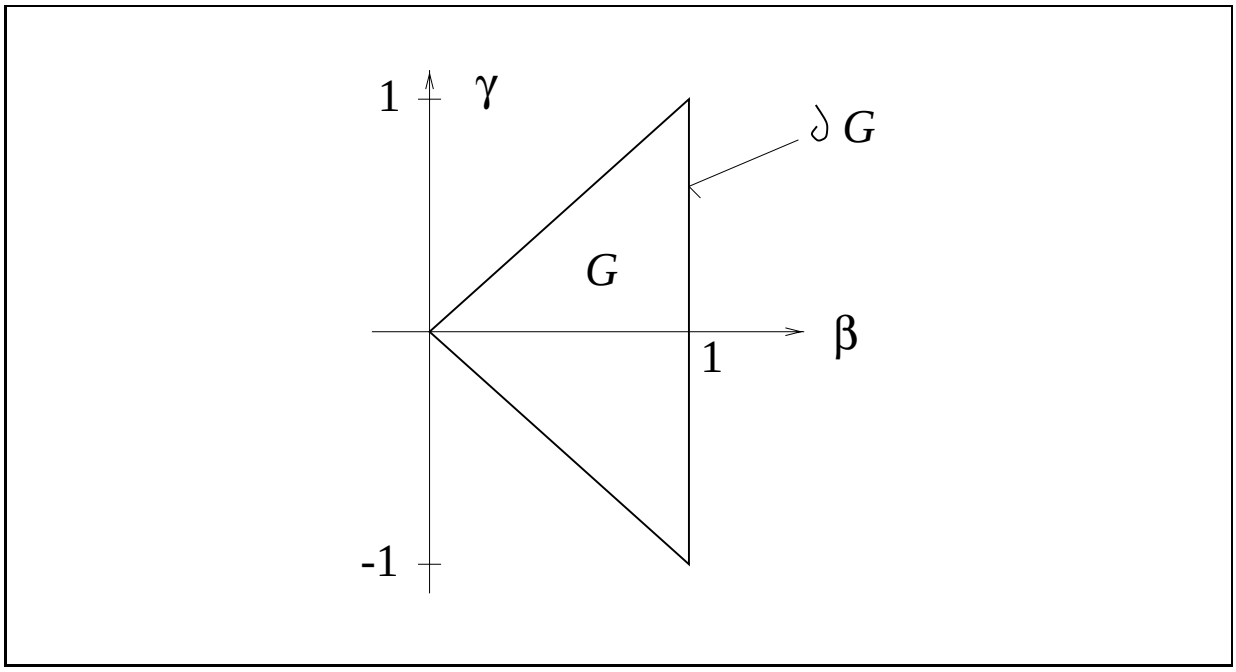

Fig. 3: The set G of admissible states G forms a triangle with its corners at (0,0), (-1,1), and (1,1).

The second internal variable γ represents the state of relative polarization associated to a degree of aligment of c axes given by β. Consequently, γ may assume values between -β and β: In the case $\gamma = \beta$, all domains within the 45° cone about the x_3 axis are polarized in positive x_3 direction while $\gamma = -\beta$ means the opposite. If $\gamma = 0$, the fractions of domains in the 45° cones polarized in positive and negative x_3 direction are equal, leading to a cancelation of the resultant remanent polarization. Especially, $\gamma = 0$ in the unpoled reference state.

In summary, we find that β and γ may take values according to

$$0 \leq |\gamma| \leq \beta \leq 1 \quad . \tag{34}$$

This means the microstructural parameters β and γ are not completely independent of each other and admissible internal states are represented by the set

$$G = \left\{ \; (\beta, \gamma) \; \middle| \; 0 \leq |\gamma| \leq \beta \leq 1 \; \right\} \quad . \tag{35}$$

As shown in the β-γ-plane in Fig. 3, G is a triangle with its corners at (0,0), (-1,1), and (1,1).

3.4 History dependent piezoelectricity

It remains to specify the dependence of the coefficients in the piezoelectricty relations (26) and (27) on the microstructural parameters β and γ. Clearly, the elastic and dielectric response of a ferroelectric is influenced by its domain state. This can easily be seen

by comparing the elastic and dielectric constants of a poled ceramic in poling direction to those obtained in perpendicular direction. Since the corresponging values differ by approximately 10 %, we may neglect the dependence of Y and ϵ on the microstructural parameters in order to keep the model as simple as possible. However, the situation is completely different for the piezoelectric coefficient $\hat{\mathrm{d}}$: In the unpoled state the phenomenon of piezoelectricity is not only modified quantitatively, it is totally absent then: $\hat{\mathrm{d}} = 0$ if $\mathrm{P^i} = 0$. In the poled state ($\mathrm{P^i} = \pm \mathrm{P_{sat}}$), the piezoelectric coefficient reaches its maximum magnitude: $\hat{\mathrm{d}} = \pm \mathrm{d_{sat}}$. For simplicity, we fit by a linear function:

$$\hat{\mathrm{d}}(\gamma) = \mathrm{d_{sat}}\, \gamma = \mathrm{d_{sat}}\, \frac{\mathrm{P^i}}{\mathrm{P_{sat}}} \tag{36}$$

We want to emphazise that concerning all functional relations for their dependence on the microstructural parameters, we tried to make the simplest choice which is still physically reasonable in a qualitative manner. We did so, since it is our primary goal to discuss the basic features of our model in this paper.

3.5 Evolution equations for the internal variables

It is the constituting feature of ferroelectric ceramics that their domain state can be changed by switching the microdipole of a unit cell by either an electric field or mechanical loads of sufficient magnitude. These mechanisms are depicted in Fig. 4. An electric field will try to give the microdipoles its own orientation. Compressive mechnical stresses acting in the direction of the c axis of a unit cell will eventually make it switch by 90°, however, it can not trigger a unique orientation of the microdipole in the new state. We now need to define evolution equations for our microstructural parameters in a way that the macroscopic consequences of these mechanisms are described.

The starting point for the introduction of our evolution equations is the Gibbs energy g from which the driving forces f_α are derived. Since the part g^{i} has not been specified yet, we now choose the following relation:

$$\rho\, g^{\mathrm{i}} = -\frac{1}{2}\, c_\beta\, (\beta - \beta_{\mathrm{ref}})^2 - \frac{1}{2}\, c_\gamma\, \gamma^2 - I_G(\beta, \gamma) \tag{37}$$

By introducing an appropriate function $I_G(\beta, \gamma)$, we have to ensure that the microstructural parameters assume admissible values from the set $G = \{\ (\beta, \gamma)\ |\ 0 \leq |\gamma| \leq \beta \leq 1\ \}$ only. Further details concerning this function will be discussed in the following sections.

The role of the two other terms in g^{i} can be seen, if we have a look at the driving forces resulting from this form of the Gibbs energy. With the help of the functions (28), (31), and (36) we find by applying the prescription (22)

$$f_\beta = \frac{S_{\mathrm{sat}}}{1 - \beta_{\mathrm{ref}}}\, \sigma - c_\beta\, (\beta - \beta_{\mathrm{ref}}) - \frac{\partial I_G}{\partial \beta} \tag{38}$$

$$f_\gamma = \mathrm{P_{sat}}\, \mathrm{E} + \mathrm{d_{sat}}\, \sigma\, \mathrm{E} - c_\gamma\, \gamma - \frac{\partial I_G}{\partial \gamma} \tag{39}$$

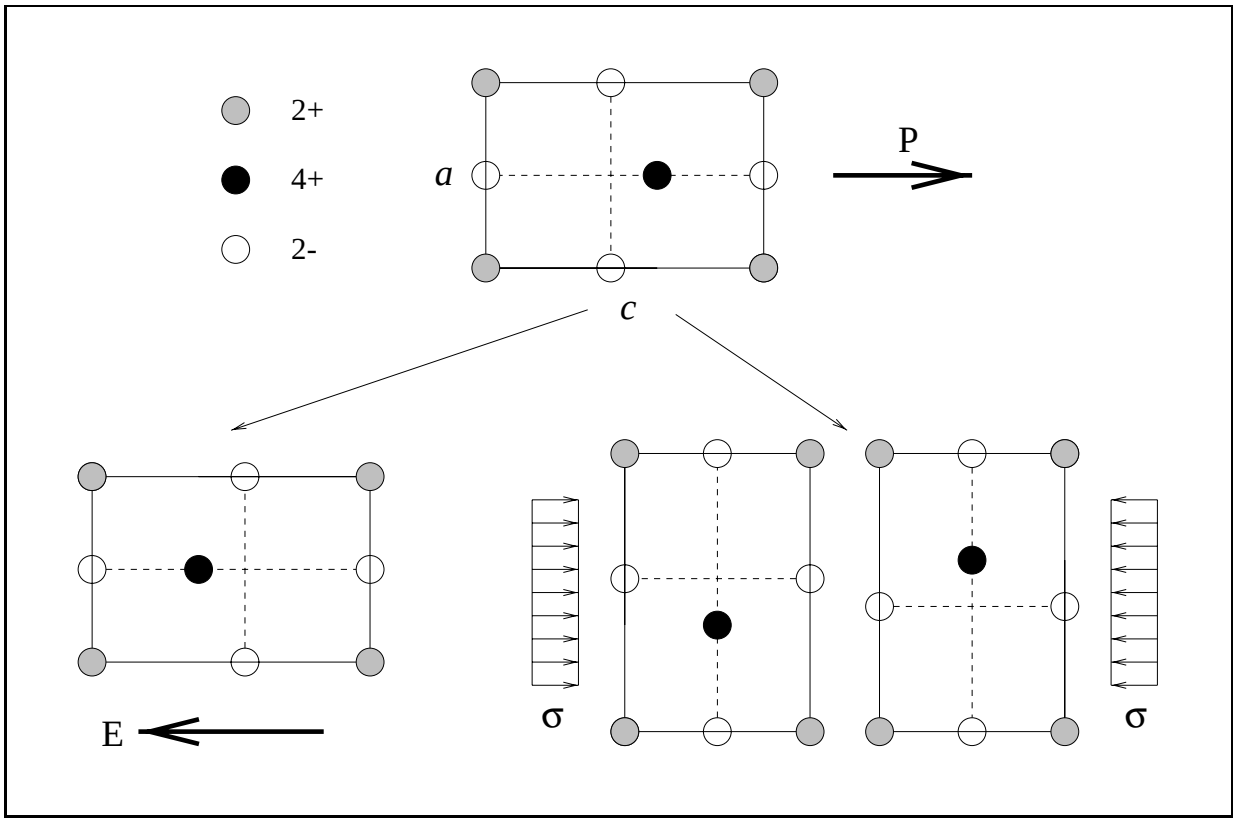

Fig. 4: Switching mechanisms in a tetragonal ferroelectric ceramic.

for the driving forces. Of course, the primary contribution to the driving forces stems from the mechanical stress and from the electric field. Now, if we assume that c_β und c_γ are non-negative constants, as we will do from now on, we see that the corresponding terms reduce the magnitude of the driving forces as the values of the microstuctural parameters grow. In this way, we represent the fact that the unpoled state is most preferred and departing from the unpoled state expieriences an increasing resistance caused by the constraint from neighbouring domains and grains.

In order to satisfy the Clausius-Duhem inequality in a sufficient manner, we now choose

$$\dot{\beta} = \Lambda \, f_\beta \tag{40}$$

$$\dot{\gamma} = \Lambda \, f_\gamma \tag{41}$$

as evoltion equations for the internal variables. In fulfillment of the requirement (23), the function

$$\Lambda = \Lambda_0 \left\langle \sqrt{f_\beta^2 + f_\gamma^2} - \mathrm{P_{sat}} \, \mathrm{E_c} \right\rangle \tag{42}$$

is non-negative (Λ_0: positive material constant, $\langle x \rangle = x$ if $x \geq 0$ and $\langle x \rangle = 0$ if $x \leq 0$). According to the function Λ, microstructure evolution takes place if the magnitude of

the total driving force reaches a critical value $\mathrm{P_{sat}E_c}$. This threshold has been chosen such that starting from the unpoled reference state ($\beta = \beta_{\mathrm{ref}}$, $\gamma = 0$), the microstructural parameters will not change under pure electric loadings as long as the magnitude of the electric field remains below the *coercitive field* $\mathrm{E_c}$. This means that we have a range of linear dielectric behavior for sufficiently small values of the electric field. In order to have irreversible poling processes, the coercitive field has to be overcome. Starting from the unpoled reference state, we find from the condition $\Lambda = 0$ for the *coercitive stress* σ_{c} necessary to initiate mechanically caused switching processes

$$\sigma_{\mathrm{c}} = \frac{1 - \beta_{\mathrm{ref}}}{S_{\mathrm{sat}}} \, \mathrm{P_{sat}} \, \mathrm{E_c} \tag{43}$$

by equations (40) and (42).

Since the right hand sides of the evolution equations (40) and (41) are functions of the state variables only, the model response shows rate effects. The choice of Λ and especially the constant Λ_0 influences this rate dependence. This can be seen by introducing the material intrinsic time scale

$$\tau = \Lambda_0 \, t \tag{44}$$

yielding

$$\dot{\beta} = \Lambda_0 \, \frac{\mathrm{d}\beta}{\mathrm{d}\tau} \tag{45}$$

$$\dot{\gamma} = \Lambda_0 \, \frac{\mathrm{d}\gamma}{\mathrm{d}\tau} \tag{46}$$

for the time derivatives of the internal variables. We see that for large values of Λ_0, time dependent processes in the material take place very rapidly on the physical time scale t. This means that we get a nearly spontaneous response without rate effects for sufficiently large values of Λ_0. On the other hand, if we choose small values for Λ_0, time processes in the material are delayed with respect to t and we expect a significant rate dependence of the model response. For further discussions of these aspects we refer to the next sections.

4 Discussion of an idealized formulation of the model

Following [41], we may choose for I_G the indicator function of the set G in order to enforce that the pair of internal variables assumes only admissible values from this set. The indicator function is defined by

$$I_G(\beta, \gamma) = \begin{cases} 0 & , \quad (\beta, \gamma) \in G \backslash \partial G \\ \infty & , \quad \text{else} \end{cases} \quad , \tag{47}$$

where ∂G is the boundary of G. As a rough physical interpretation, we may state that the indicator function surrounds the set of admissible values of (β, γ) by an infinitely steep

and infinitely high energy barrier. As long as (β, γ) takes values in the interior of G, there is no contribution from the indicator function to the driving forces. However, as soon as the (β, γ) is situated on the boundary of G, the contribution from the indicator function to the driving forces will be such that no values outside G can be reached. We consider this step like behavior induced by the use of the indicator function as an idealized way to enforce the constraints for physically admissible values of the microstructural parameters.

Instead of using the mathemetical formulation of [41] employing convex analysis, we adopt the represention of the indicator function found in [42]. Introducing the functions

$$h_1(\beta, \gamma) = \gamma - \beta \tag{48}$$

$$h_2(\beta, \gamma) = -\gamma - \beta \tag{49}$$

$$h_3(\beta, \gamma) = \beta - 1 \tag{50}$$

the set G may be represented equivalently by

$$G = \left\{ (\beta, \gamma) \,\middle|\, h_i(\beta, \gamma) \leq 0 \ , \ i = 1, 2, 3 \right\} \quad . \tag{51}$$

The indicator function may then be written as

$$I_G(\beta, \gamma) = -\lambda_1 h_1 - \lambda_2 h_2 - \lambda_3 h_3 \quad . \tag{52}$$

Adopting for the remainder of this paper the approximate value $\beta_{\text{ref}} = \frac{1}{3}$, this yields the evolution equations

$$\dot{\beta} = \Lambda \left(\tfrac{3}{2} \, S_{\text{sat}} \, \sigma - c_\beta \, (\beta - \tfrac{1}{3}) + \lambda_1 + \lambda_2 - \lambda_3 \right) \tag{53}$$

$$\dot{\gamma} = \Lambda \left(\mathrm{P}_{\text{sat}} \, \mathrm{E} + \mathrm{d}_{\text{sat}} \, \sigma \, \mathrm{E} - c_\gamma \, \gamma - \lambda_1 + \lambda_2 \right) \tag{54}$$

Here, the multipliers λ_i satisfy the Kuhn-Tucker conditions

$$h_i \leq 0 \quad , \quad \lambda_i \geq 0 \quad , \quad h_i \lambda_i \leq 0 \qquad , \qquad i = 1, 2, 3 \quad . \tag{55}$$

It might be interesting to shed some light on the role of the λ-terms in the driving forces. For values of microstructural parameters from the interior of G, i. e. $(\beta, \gamma) \in G \backslash \partial G$, we find $h_i < 0$, $i = 1, 2, 3$. According to the Kuhn-Tucker conditions (55), the driving forces are then given by the "regular" parts

$$f_\beta = f_{\beta \text{reg}} = \tfrac{3}{2} \, S_{\text{sat}} \, \sigma - c_\beta \, (\beta - \tfrac{1}{3}) \tag{56}$$

$$f_\gamma = f_{\gamma \text{reg}} = \mathrm{P}_{\text{sat}} \, \mathrm{E} + \mathrm{d}_{\text{sat}} \, \sigma \, \mathrm{E} - c_\gamma \, \gamma \tag{57}$$

Now, lets assume that (β, γ) is on the boundary $\beta = \gamma$ of G, i. e. $h_1 = 1$. If at this state

$$\left. \frac{\mathrm{d} h_1(\beta, \gamma)}{\mathrm{d} t} \right|_{f_\beta = f_{\beta \text{reg}}, f_\gamma = f_{\gamma \text{reg}}} > 0 \quad , \tag{58}$$

the multiplier $\lambda_1 > 0$ has to be chosen according to the Kuhn-Tucker conditions (55) such that the pair (β, γ) doesn't get outside the set of admissible values, i. e. $h_1(\beta, \gamma) \not> 0$. From the consistency condition

$$\left.\frac{\mathrm{d}h_1(\beta,\gamma)}{\mathrm{d}t}\right|_{f_\beta = f_{\beta\,\mathrm{reg}} + \lambda_1, f_\gamma = f_{\gamma\mathrm{reg}} - \lambda_1} = 0 \tag{59}$$

we find

$$\lambda_1 = \frac{1}{2}\left(- f_{\beta\mathrm{reg}} + f_{\gamma\mathrm{reg}}\right) \quad . \tag{60}$$

Consequently, the evolution equations are given by

$$\dot{\beta} = \Lambda \frac{1}{2}\left(f_{\beta\mathrm{reg}} + f_{\gamma\mathrm{reg}}\right) \tag{61}$$

$$\dot{\gamma} = \Lambda \frac{1}{2}\left(f_{\beta\mathrm{reg}} + f_{\gamma\mathrm{reg}}\right) \tag{62}$$

in this situation. Obviously, $\dot{\beta}/\dot{\gamma} = 1$ now, meaning that the term λ_1 corrects the driving forces such that the state (β, γ) may move along the boundary $h_1 = 1$ of G but cannot get outside. Instead of going futher in the mathematical details of this particular aspect of our model, we now turn to discuss the physical significance of the model by considering its response to characteristic electro-mechanical loading paths.

ϵ	mC/kV m	0.05	Y	MPa	100
$\mathrm{d_{sat}}$	mm/kV	0.001	S_{sat}	%	0.3
$\mathrm{E_c}$	kV/mm	1.0	$\mathrm{P_{sat}}$	$\mathrm{mC/m^2}$	300

Tab. 1: Values of the classical ferroelectric material constants chosen for the numerical calculations in this paper.

While the physical meaning of most of the material constants in our model is clear, this is not so obvious for some of them. In particular the piezoelectric constants as well as the coercive field, the saturation polarization and the saturation strain can be measured by standardized methods. For the remainder of this paper, we choose their values according to table 1 in a way that they are charactersitic for typical ferroelectric ceramics without representing a single composition precisely. The other parameters, i e., Λ_0, c_β, and c_γ which are typical of our model are varied in the calcutions in order to demonstrate their role.

4.1 Poling and electrical cycling

The probably most commonly investigated type of loading of ferroelectric ceramics is poling and cycling by strong electric fields. Under these loadings, the typical dielectric hysteresis and the butterly hysteresis occur. We consider electric cycling with an amplitude of twice the coercive field, i. e., 2.0 kV/mm.

a) b)

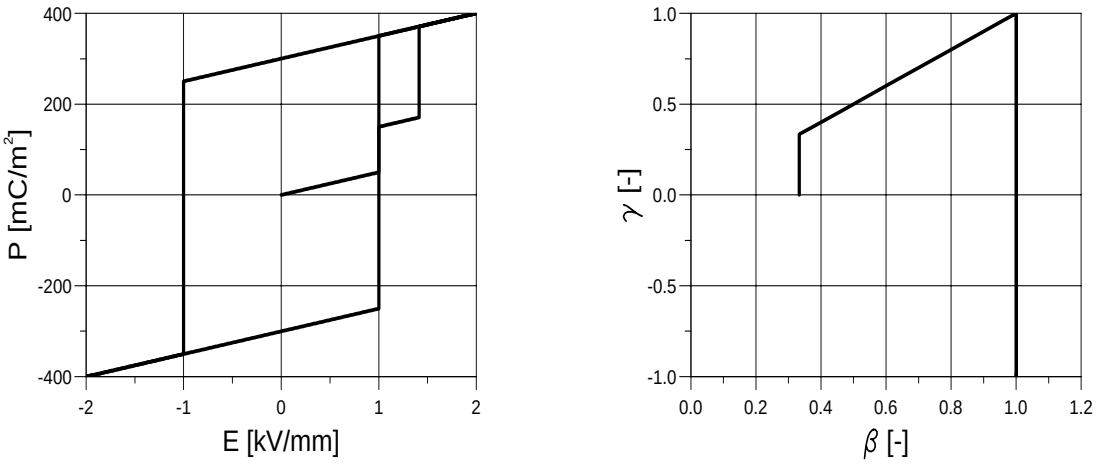

Fig. 5: Model response to a cyclic electric field (saw tooth shape) of ± 2.0 kV/mm amplitude for zero c_β and c_γ. Λ_0 has been chosen large in order to get a spontaneous model response.
a) Dielectric hysteresis
b) β-γ plane

4.1.1 Rate independent response for zero values of c_β and c_γ

To begin with, we are interested in the spontanous model response for zero values of c_β and c_γ. This investigation is to make us familiar with the basic features of our model before we get into refinement of the model response by choosing more realistic values for the material parameters c_β, c_γ, and Λ_0. In the first step, we consider the dielectric hysteresis in Fig. 5a) and the corresponding trajectory of (β, γ) in Fig. 5b). The polarization is computed according to the additive decomposition (25) and the relations (27) and (33) for the reversible and irreversible parts, respectively:

$$\mathrm{P} = \epsilon \mathrm{E} + \mathrm{P}_{\mathrm{sat}}\,\gamma \tag{63}$$

As long as the electric field is below the coercive field of 1.0 kV/mm, we observe in Fig. 5a) a linear dielectric response where the slope is given by ϵ. (β, γ) remain at their initial values $(\frac{1}{3}, 0)$. At $\mathrm{E} = \mathrm{E_c}$, Λ becomes non-zero and the growth of the internal variables starts. In Fig. 5b), we observe that γ starts to grow while β remains at its initial value since the driving force f_β is still zero. Because Λ_0 has been given a large value in order to yield a spontaneous model response, the growth of γ is very rapid. (For values above $\Lambda_0 = 2.0 \cdot 10^{-2}$ sec^{-1}·kPa^{-2}, the model response showed no rate effets.) This can be seen from the step like increase of the polarization to a value of 171 mC/m^2 in Fig. 5a) due to the corresponding increase of $\mathrm{P^i}$ related by equation (33).

According to the microscopic interpretation of the microstructural parameters, the model response in this period of the loading history may be considered representing pure 180° switching processes: The state of the c axes described by β remains constant while the relative polarization, i e., the orientation of the microdipoles changes. At $\gamma = \frac{1}{3}$, all microdipoles within the 45° cones about the axis of poling are oriented in the direction of the electric field and the reservoir for pure 180° switching is gone.

At $(\beta, \gamma) = (0, \frac{1}{3})$, the boundary ∂G of admissible values for the internal variables is reached, indicated by $h_1 = 0$. Due to the electric field, the driving force $f_{\gamma \mathrm{reg}}$ continues growing. However, a further increase of γ is only admissible if it is compensated by a corresponding growth of β. In fact, as we have seen in the discussion prior to this subsection, the indicator function $I_G(\beta, \gamma)$ defined in equation (52) provides corrective terms to the driving forces.

At the incident of their occurence, these correction terms cause a drop of the magnitude $\sqrt{f_\beta^2 + f_\gamma^2}$ of the total driving force, resulting $\sqrt{f_\beta^2 + f_\gamma^2} < \mathrm{P_{sat}E_c}$. Therefore, the evolution of the internal variables stops, and changes of P are linear with ϵ as the slope, until $\sqrt{f_\beta^2 + f_\gamma^2}$ reaches the critical value $\mathrm{P_{sat}E_c}$ again due to the continued growth a the electric field.

This pause in the evolution of the microstructural parameters can be associated readily to the higher energy level needed to initiate 90° switching processes compared to 180° switching: As we have seen before, further polarization switching beyond the state $(\beta, \gamma) = (0, \frac{1}{3})$ is possible only, if accompanied by changes of β representing the state of the c axes. However, in its microscopic interpretation, such a changes mean 90° switching. Now, since 90° switching causes a strain mismatch in the crystal structure, the neighbourhood of the unit cells to be switched acts as resisting contraint and a higher energy level is needed compared to 180° switching

Once the critical load for further irreversible evolution is reached again at E = 1.4 kV/mm, (β, γ) attain spontaneously their limiting values $(1, 1)$. According to equation (33), $\mathrm{P^i}$ jumps to the value $\mathrm{P_{sat}}$ yielding the second step observed in the dielectric hysteresis in Fig. 5a).

By the value $(1, 1)$, our microscopic parameters represent a state where all c axes are situated within the 45° cone about the axis of poling ($\beta = 1$), with all microdipoles oriented to the positive $\mathrm{x_3}$ axis which is the current orientation of the electric field ($\gamma = +1$). In its microscopic interpretation, this is the fully poled state. This fully poled state provides no further reservoir of switchables domains for ongoing poling in the same direction as before even if the electric field keeps on increasing.

This is reflected by the fact that the pair $(1, 1)$ is the outermost corner of the triangle G of admissible values of (β, γ), see Fig. 3. Any further increase of the electric field is offset by correction terms due to the indicator function I_G leading to vanishing driving forces. A microscopic interpretation for this behavior is that the domain structure after having been fully switched exhibits resistance needed to prevent any further switching. This resistance annihilates the agitation by the electric field.

The increase of P is now linear again, with ϵ as the slope. Note that due to our isotropy assumption for ϵ, i. e., its independence of the microstructural parameters, the slopes of

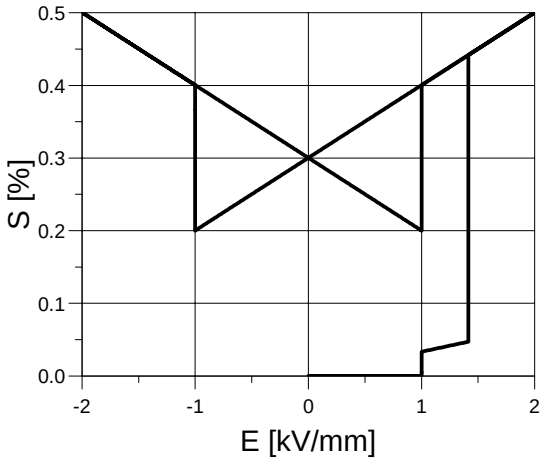

Fig. 6: Butterfly hysteresis corresponding to the curves in Fig. 5.

the unpoled and the fully poled portions of the dielectric curve in Fig. 5a) are equal.

Before we continue the discussion of the dielectric properties, we now consider the poling part of the butterfly hysteresis in Fig. 6, i. e., the strain induced by a poling electric field. It can be calculated by the additive decomposition (24) and the relations (26) and (31) for the reversible and irreversible parts, respectively, yielding

$$S = \mathrm{d}_{\mathrm{sat}}\,\gamma\,\mathrm{E} + \tfrac{3}{2}\,S_{\mathrm{sat}}\,(\beta - \tfrac{1}{3}) \quad , \tag{64}$$

if we choose $\beta_{\mathrm{ref}} = \frac{1}{3}$ and $\hat{\mathrm{d}}$ according to (36).

Starting from the thermally depoled reference state, there is no electro-mechanical coupling in the macroscopic ceramic. As soon as the coercive field is reached, we observe a small jump in the induced strain corresponding to the first jump of P at $\mathrm{E} = \mathrm{E_c}$ in the dielectric plot Fig. 5. This strain cannot be associated to 90° switching since β remains at its initial value $\frac{1}{3}$ so far. Rather, this strain is due to the piezoelectric effect caused by a net polarization induced by 180° switching and the acting electric field. The step like character of the strain evolution is connected to the spontaneous growth of γ.

During the following pause of the evolution of the internal variables, the strain varies linearly with the electric field. The slope is given by the current value $\mathrm{d}_{\mathrm{sat}}\frac{1}{3}$ of the piezoelectric coefficient of E in the first term of equation (64). This means that the piezoelectric effect is already present to a certain extent in this partially poled state.

As soon as the barrier for 90° switching is overcome at $\mathrm{E} = 1.4$ kV/mm, β and γ increase spontaneously to their limiting value 1, as discussed before. According to equation (64) this leads to a related jump of S due to both its piezoelectric and irreversible parts. This second jump is larger then the first one because of the impact of 90° switching on the irreversible strain. From then on, we have a pure linear piezoelectric response of the fully poled state.

We now come back to the dielectric hysteresis in Fig. 5a). After the electric field has reached its maximum value of 2.0 kV/mm, it is first reduced to zero and then reversed to -2.0 kV/mm. During unloading, we observe a linear dielectric model response. At E = 0 kV/mm, we read an irreversible, i.e., remanent polarization of P = P_{sat} = 300 mC/m^2 from the plot in Fig. 5a).

At E = −1 kV/mm, Λ reaches its critical value and the internal variables may be subject to change again, this time starting from $(1, 1)$. The electric field and thus the driving force $f_\gamma = f_{\gamma\text{reg}}$ act now in the negative x_3 direction while $f_\beta = f_{\beta\text{reg}}$ vanishes. Consequently, the total driving force $(f_\beta, f_\gamma) = (f_{\beta\text{reg}}, f_{\gamma\text{reg}})$ points along the border of G, but not to its exterior and because of this, no correction by additional terms due to the indicator function I_G will occur. γ changes spontaneously from +1 to -1, while β is constant, since its driving force is zero during this period, see Fig. 5b). At $(\beta, \gamma) = (1, -1)$, the boundary ∂G is reached again and because the total driving force $(f_{\beta\text{reg}}, f_{\gamma\text{reg}})$ now points to the exterior of G, the indicator function kicks in to maintain the internal variables in the range of admissible values, i.e., at $(1, -1)$. Due to the change of γ from 1 to -1, we observe a complete reversion of the polarization to second fully poled state. After unloading we find a remanent polarization of P = $-P_{sat}$ = −300 mC/m^2

In its microscopic interpretation, this polarization reversal is related to pure 180° switching without 90° switching: The fact that β is constant at a value of 1 means that all c axes remain within the 45° cones about the axis of loading. The change of γ alone has to be associated to a pure reorientation of the microdipoles within these cones from the old to the new direction of the electric field. This interpretation is consistent with the absence of a pause of the evolution of the internal variables like the one observed during the poling process starting from the depoled reference state $(\frac{1}{3}, 0)$. Starting from the fully poled state, all domains can switch to the new orientation of the electric field in one step by 180°. There is no need to assume energetically less favorable intermediate states by 90° switching.

Looking at the butterfly hysteresis in Fig. 6, we observe during unloading a linear piezoelectric response leaving a remanent strain of $S = S_{sat} = 0.3\%$. The spontaneous process of repoling finds its expression in the observation of a jump in the induced strain at E = −1.0 kV/mm. At this intstant, the piezoelectric coefficient in equation (64) changes its sign and the piezoelectric strain instead of being subtracted from S_{sat}, is now added to it. A second piezoelectric range with opposite sign but otherwise equivalent behavior is reached. No change at all occurs in the second term of equation (64) since β is constant.

From a microscopic point of view, it is clear that pure 180° switching causes no change of the remanent strain. Only the strain induced by an electric field via the piezoelectric effect is affected due to the reversal of the net polarization: The piezoelectric strain changes its sign.

4.1.2 Discussion of c_β and c_γ

The step-like switching behavior in Fig. 5 is usually attributed to single crystals where no neighborhood of misoriented grains constrains the simultaneous switching of all mi-

a) b)

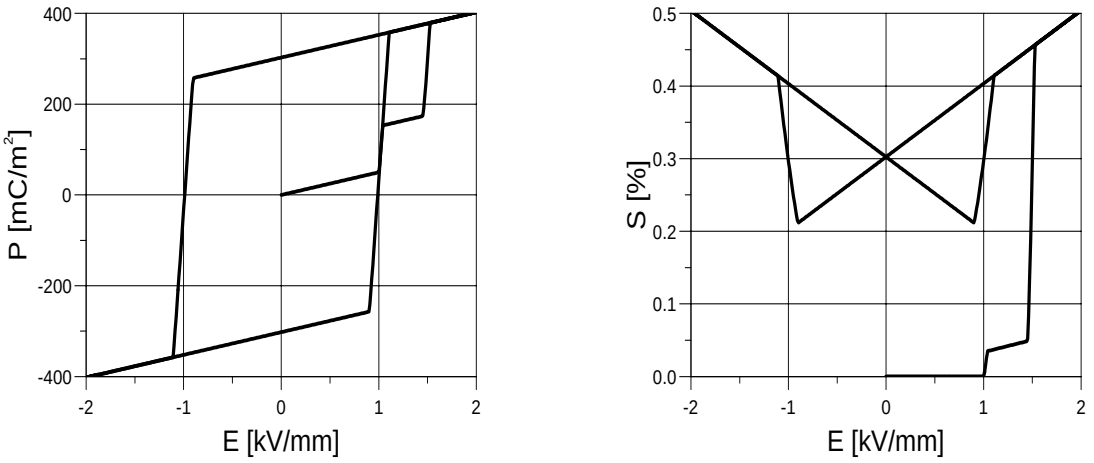

Fig. 7: Model response to a cycling electric field for $c_\beta = 0.0$ kPa and $c_\gamma = 30.0$ mC/m^2 $\cdot$ kV/mm:
a) Dielectric hysteresis
b) Butterfly hysteresis

crodipoles. However, in a polycrystalline and multidomain ceramic composed of numerous misoriented grains and containing defects this idealized kind of behavior is not observed. Rather, the polarization grows steadily as the electric field has to overcome gradually the increasing resistence of the lattice structure of the ceramic against the progressive ordering during poling.

In order to represent this internal resistence of the microstructure, we have introduced a limiting term in each of the driving forces f_β and f_γ in equations (38) and (39), respectively. Due to this term, a counter force proportional to the value of the corresponding internal variable itself is built up as it departs from its initial value in the reference state. The factors of proportionality of these terms are denoted by c_β and c_γ, respectively.

To begin with, we consider the influence of c_γ on the model response by choosing $c_\gamma = 30.0$ mC/m^2 $\cdot$ kV/mm, and leaving $c_\beta = 0.0$ kPa. Figs. 7a) and b) show the resulting dielectric hysteresis and butterfly hysteresis, respectively. The path of microstructural evolution in the β-γ plane is not shown, since it is exactly the same as in Fig. 5b). As the main difference we now observe in the dielectric plot a finite slope of the polarization over the electric field during poling. Furthermore, the magnitude of the critical value of the electric field for repoling at reversal of the electric field is reduced below $\mathrm{E_c}$. Otherwise, the basic features of the hysteresis are the same as before.

Likewise, we recognize finite slopes in the butterfly hysteresis during poling too. The curvature of the plot during poling is due to the fact that both the piezoelectric coefficient and the electric field in the first term of the strain relation (64) change in these periods.

Next, we study the role of c_β by taking $c_\beta = 100.0$ kPa, and $c_\gamma = 0.0$ mC/m^2 $\cdot$ kV/mm.

a) b)

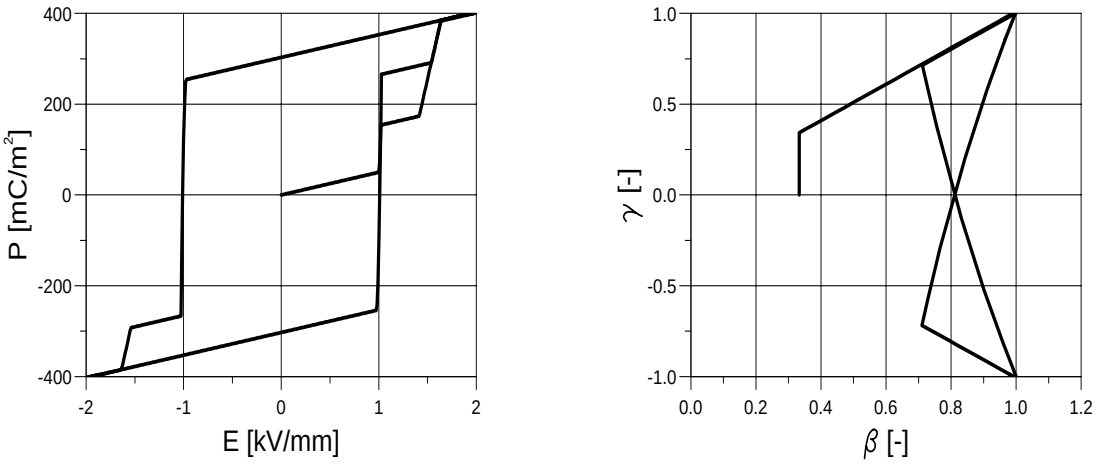

Fig. 8: Model response to a cycling electric field for $c_\beta = 100.0$ kPa and $c_\gamma = 0.0$ mC/m^2 · kV/mm:
a) Dielectric hysteresis
b) β-γ plane

Since the counter force term in f_γ is not active now, we observe during the first period of 180° switching the same spontaneous poling behavior as in Fig. 5a). In the second period of poling, which is accompanied by 90° switching, β departs from its starting value and thus the counter force term in f_β is activated. As a result, we find a finite slope of the polarization over the electric field now.

The most significant difference with respect to the previous behavior, however, is observed during reversing the electric field in Fig. 8b). In contrast to the situations considered before, $f_{\beta\mathrm{reg}} = -c_\beta(\beta - \frac{1}{3})$ now causes a partial reduction of β until the boundary of G is hit again due to $|\gamma| = \beta$. Then, the indicator function I_G dominates f_β once more and a further change of γ is compensated by an increase of β, such that (β, γ) take only admissible values. As a result of this intermediate decrease of β followed by a newly increase as γ changes from one fully poled state to the other, the β-γ curve exhibits a butterfly like shape.

This partial recovery of β during field reversal can be interpreted microscopically as back switching of such 90° domains that have been forced to align with the axis of loading only by very high fields against a resisting neighborhood. As the electric field is reversed, these domains are driven back to their original 90° state by the constraint due to the mismatch of neighboring grains and domains, before they are oriented in the new direction of the electric field by a second step of 90° switching.

Consequently, the response during repoling is different compared to the previous cases, since now both 180° and 90° switching processes occur. After reaching $\mathrm{E} = -\mathrm{E_c}$, the polarization changes by a severe jump similar to the one in Fig. 5a) due to a sudden increase

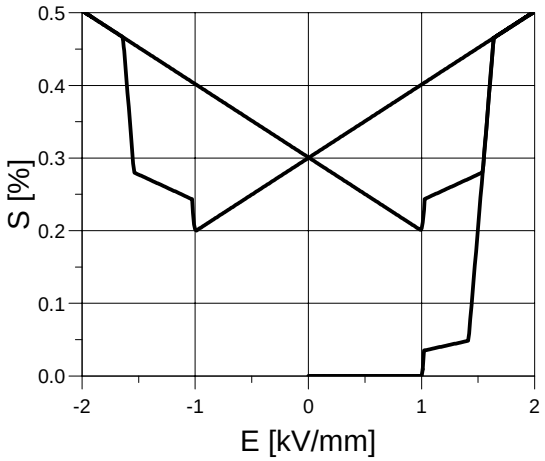

Fig. 9: Butterfly hysteresis for $c_\beta = 100.0$ kPa and $c_\gamma = 0.0$ mC/m^2 $\cdot$ kV/mm

of γ. However, this time, the boundary of G, i.e., $|\gamma| = \beta$, is reached before the magnitude of γ takes its saturation value 1, see Fig. 8b). The indicator function I_G is activated to modify the driving forces such that only admissible values of the internal variables occur. Due to this modification of the driving forces $\sqrt{f_\beta^2 + f_\gamma^2}$ drops below its critical value $\mathrm{P_{sat}E_c}$ and just as during the first poling from the reference state, the evolution of the internal variables experiences a pause. Again, this pause might be interpreted microscopically as the need to overcome a higher energy barrier related to 90° switching. The critical value for the second onset of poling is reached as the first polarization curve is met. (This can be observed during repoling from $\mathrm{E} = -2.0$ kV/mm to $\mathrm{E} = 2.0$ kV/mm.) Since the recovery of β during repoling stops well above the reference value, the second step of 90° switching is smaller then the one during poling from the reference state.

Now β is no longer constant during repoling, and because of this the irriversible strain S^{i} in the second term of equation (64) changes as well as the piezoelectric term. This is of course consistent with the microscopic interpretation relating β to 90° domains. In fact, we obtain the significantly modified butterfly hysteresis shown in Fig. 9. The difference with repect to Fig. 6 occurs during the first polarization and during repoling. In the second step of the first polarization curve representing 90° switching, we now observe a finite slope of the strain over the electric field. After the reversed electric field has passed the critical value $\mathrm{E_c}$, the switching of γ stops at $|\gamma| = \beta$ as discussed before. During the following pause of the internal variables, we have a pure linear piezoelectric changing of the strain. The slope is smaller then in the fully poled state since γ in the piezoelctric coefficient is below its saturation value 1. As the first polarization curve is met, the second step of 90° poling takes place until a fully poled state ($\gamma = 1$) with linear piezoelectric behavior is reached.

In Fig. 10, we see the combined effect of non-zero values for c_β and c_γ (the β-γ plane

a) b)

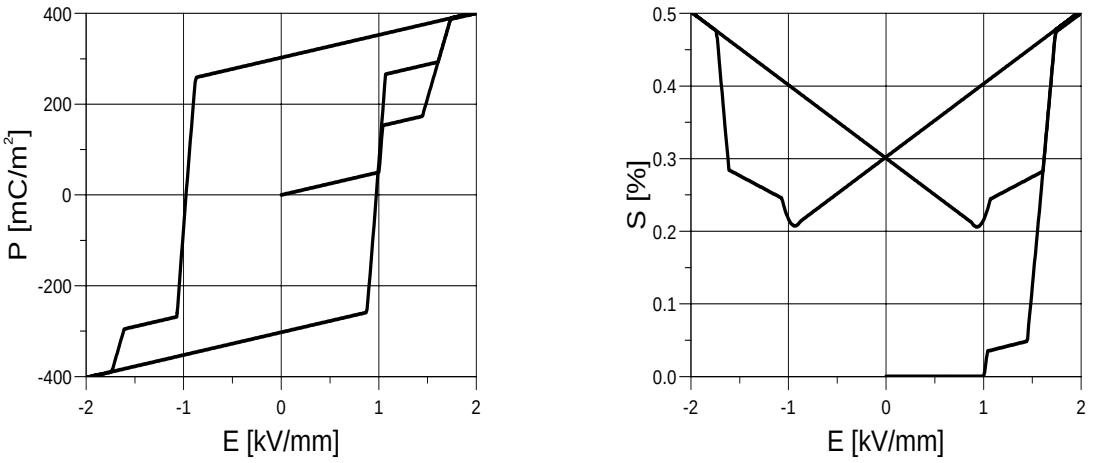

Fig. 10: Model response to a cycling electric field for $c_\beta = 100.0$ kPa and $c_\gamma = 30.0$ mC/m^2 $\cdot$ kV/mm:
a) Dielectric hysteresis
b) Butterfly hysteresis

has not been reproduced, since it is identical to the one shown in Fig. 9b)). Basicly, these curves exhibit the superposed effects discussed above for the two special cases. All in all, we recognize clearly a more realistic model response due to the presence of counter force terms in the driving forces. Their microscopic motivation has been given at the beginning of this section.

4.1.3 Rate dependence

It is well known that ferroelectric ceramics exhibit significant rate dependence effects. Especially in the case of so-called hard-PZT, the diffusion of ions gives rise to typical time constants for the electro-mechanical properties of the ceramic. Because of this, the change of the macroscopic properties of the ceramic due to a change of the external loads is not completely spontaneous. Rather, at least part of the material response is delayed leading to relaxation phenomena.

Until now, we chose $\Lambda_0 \geq 2.0 \cdot 10^{-2}$ sec^{-1}·kPa^{-2} in order to get a sponateous model response. Fig. 11 shows the model response computed for $\Lambda_0 = 1.0 \cdot 10^{-3}$ sec^{-1}·kPa^{-2} ($c_\beta = 100.0$ kPa, $c_\gamma = 30.0$ mC/m^2 $\cdot$ kV/mm). The hystereses now have a more curved appearence. Compared to the corresponding curves in Fig. 10, it takes larger magnitudes of the electric field to yield the same polarization value. Especially, as the eletric field reaches the peak value +2.0 kV/mm for the first time, the fully poled state $\gamma = 1$ has not yet been assumed. The polarization growth is finished during the very first period of the reduction of the electric field.

a) b)

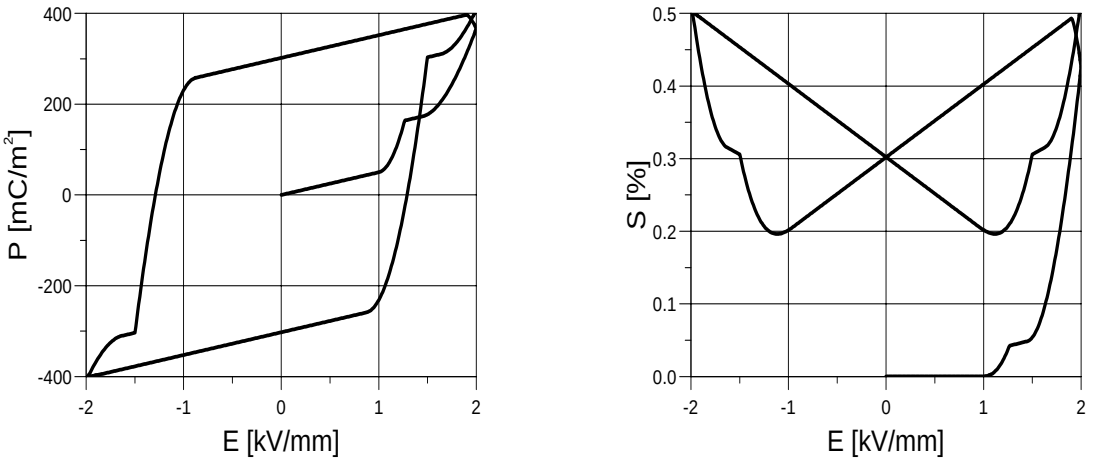

Fig. 11: Rate effects in the model response for $\Lambda_0 \geq 1.0 \cdot 10^{-3}$ sec^{-1}·kPa^{-2}:
a) Dielectric hysteresis
b) Butterfly hysteresis

Similar to equation (44), we may introduce a material intrinsic time scale by

$$\tau = \Lambda\, t \quad . \tag{65}$$

From this definition, we recognize a highly nonlinear rate dependence of our model: Besides the material constant Λ_0, the relaxation times depend on the current values of the driving forces. However, as we have seen, the basic properties of our model are determined by its spontaneous behavior. Therefore we focus on the investigation of spontaneous properties in the remainder of this paper and will not go into a further discussion its rate dependence.

4.2 Spontaneous response to mechanical compression-tension loading

Another common experiment for the macroscopical investigation of ferroelectric ceramics involves mechanical compression of samples of brick-like geometry. We consider here a complete loading cycle of initial compression loading, follow by unloading and tensile reloading. The loading cycle is closed by a final compression loading. The amplitude of the prescribed stress is 100 MPa. The material parameters were chosen according to Tab. 1. Furthermore, we took $c_\beta = 100.0$ kPa, $c_\gamma = 30.0$ mC/m^2 · kV/mm, and a sufficiently large value for Λ_0 in order to get a rate independent model response.

As we have seen before, domain switching in ferroelectric ceramics may also be induced by mechanical stresses. Since mechanical stresses can not trigger a unique orientation of

a) b)

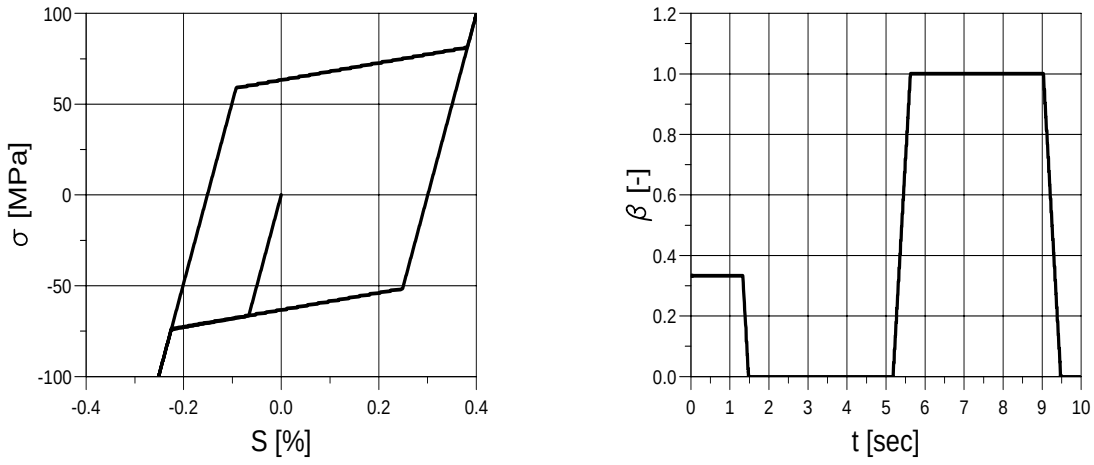

Fig. 12: Model response to pure mechanical loading:
a) Ferroelastic hysteresis
b) β as a function of t

the microdipoles, they can not lead to a net polarization of an initially unpoled sample. The sample will remain unpoled even if the domain structure is changed dramatically and thus it will exhibit no electro-mechanical coupling effects.

Starting from an unpoled state, γ will vanish identically under pure mechanical loadings, since the driving force f_γ is zero in this case, thus reflecting the above mentioned electro-mechanically decoupled behavior. The strain is computed from the additive decomposition (24) and the relations (26) and (31) for the reversible and irreveresible parts, respectively, yielding for the present situation ($\beta_{\text{ref}} = \frac{1}{3}$)

$$S = \frac{1}{Y}\,\sigma + \tfrac{2}{3}\,S_{\text{sat}}\,(\beta - \tfrac{1}{3}) \quad . \tag{66}$$

The ferroelastic hysteresis of the stress-strain behavior resulting from our loading history is shown in Fig. 12a) and the corresponding history of β is plottet in Fig. 12b). The probably most significant feature of the curves in Fig. 12 is their lack of symmetry.

At the beginning of the compression loading, we see in Fig. 12a) a linear elastic response, until the stress reaches the critical value

$$\sigma = -\sigma_{\text{c}} = -66.6 \text{ MPa} \tag{67}$$

determined by equation (43). Starting from this point, we observe irreversible ferroelastic deformation as β is reduced from its initial value $\frac{1}{3}$ to zero, see Fig. 12b). The tangent modulus, i.e., the slope of the stress-strain curve in this period depends on the value of c_β. In particular, a zero value of c_β would give a vanishing tangent modulus.

At $\beta = 0$, the boundary of the set of admissible values for the internal variables is hit, see Fig. 3. Since $(0,0)$ happens to be the corner of the triangle G corresponding to the smallest value allowed for β, its evolution is stopped by the indicator function I_G even though $f_{\beta\mathrm{reg}}$ is still increasing. In its microscopic interpretation, the state $(\beta,\gamma) = (0,0)$ corresonds to a situation where no c axes are left in the 45° cones about the axis of loading ($\beta = 0$), i e., all c axes are situated as close as possible to a plane perpendicular to the stress with no net polarization ($\gamma = 0$).

At this state, a second region of linear elastic behavior is reached. The slope of this region is the same as the initial slope, since we have assumed that Young's modulus Y is independent of the microstructural parameters, similar as we have done for ϵ. After unloading, we recognize a remanent strain of

$$S = S^{\mathrm{i}} = -\tfrac{1}{2} S_{\mathrm{sat}} = -0.15\% \quad . \tag{68}$$

Now, as a tensile stress is applied, eventually irreversible deformation starts again. β grows from 0 to 1, passing its initial value $\frac{1}{3}$ at $\sigma = \sigma_{\mathrm{c}}$. At $\beta = 1$, the boundary of G is hit and β can not grow further. This time, the magnitude of the maximum irreversible deformation is much larger as we see after linear elastic unloading. In fact, we get

$$S = S^{\mathrm{i}} = S_{\mathrm{sat}} = 0.3\% \tag{69}$$

now. This lack of symmetry of the ferroelastic hysteresis is in accordance with microscopic considerations: In a tetragonal ceramic starting from an unpoled state, the reservior of domains switchable towards the axis of loading is about twice as large as the reservoir of domains switchable perpendicular to it. It must be noted though that under tensile stresses a completely switched state is usually not attainable as specimens have the tendency to fail earlier then under compressive stresses (see [40]).

4.3 Mechanical depolarization

A critical property for the application of piezoceramics in heavily loaded actuators is the mechanical depolarization behavior of the material. If a prepoled sample is loaded by strong compressive stresses in the direction of poling, domain switching will start. However, as mentioned before, mechanical stresses can not trigger a unique orientation of the switched microdipoles and the net polarization of the sample is lost gradually as switching carries on. Loss of net polarization goes of course along with loss of piezoelectricity, making the ceramic useless for electro-mechanical applications until it is poled again.

Fig. 13 shows the reproduction of these experimental findings by our model. The material parameters were given the same values as before. The loading history consists of electrical poling by raising the electric field from zero to 2.0 kV/mm. After removing the electric field, a compressive mechanical stress up to -200.0 MPa is applied.

The poling process has already been discussed in detail in section 4.1, see Fig. 5. We recognize its effect from the horizontal line in Fig. 13a). At the peak value of the electric field, a polarization of over 400 mC/m^2 is reached. Upon removing the electric field, only

a) b)

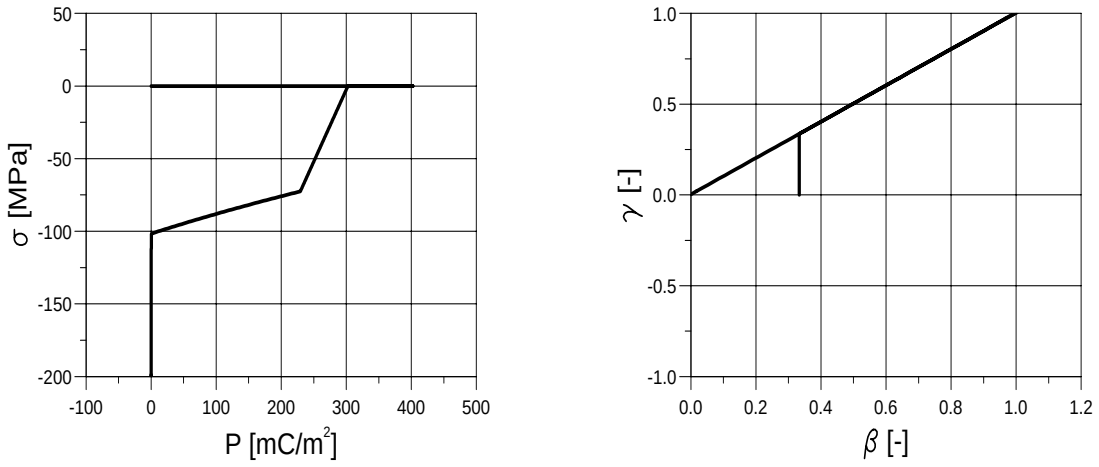

Fig. 13: Mechanical depolarization of a fully poled state:
a) Polarization vs. stress
b) β-γ plane

the remanent polarization of 300 mC/m^2 remains. This fully poled state is attained by 180° and 90° switching and is represented by $(\beta, \gamma) = (1, 1)$, see Fig. 13b).

Now, as the compressive stress is applied, we observe a linear piezoelectric response in Fig. 13a) departing from $\mathrm{P} = \mathrm{P}_{\mathrm{sat}}$. Eventually, the stress reaches a limit where $\sqrt{f_\beta^2 + f_\gamma^2}$ becomes equal to $\mathrm{P}_{\mathrm{sat}}\mathrm{E}_{\mathrm{c}}$ and the evolution of the internal variables is activated. Starting from $(1, 1)$, the driving force $(f_{\beta\mathrm{reg}}, f_{\gamma\mathrm{reg}})$ points to the exterior of the set G of admissible values of (β, γ), since $f_{\beta\mathrm{reg}}$ is negative and $f_{\gamma\mathrm{reg}}$ vanishes. Therefore, the reduction of β caused by the mechanical stress in the driving force (38) is compensated by a corresponding reduction of γ due to the indicator function I_G, in order to ensure that the internal variables take admissible values. In this way, γ is reduced to zero together with β following the border ∂G from $(1, 1)$ to $(0, 0)$. The depoled state $(\beta, \gamma) = (0, 0)$ has already been discussed in the previous section. According to equation (36) it exhibits no piezoelectric coupling.

It is interesting to consider the influence of a bias electric field on the stress level necessary for the onset of depolarization. A field with the same orientation as the polarization stabilizes the domain structure and makes a higher critical stress necessary for depolarization. On the other hand, an electric field oriented opposite to the polarization will lead to an early onset of depolarization even if it is too weak to cause domain switching by itself. According to [26], the dependence of the critical stress for depolarization on a bias field acting during the application of the compressive load is linear. From the values plotted in Fig. 14 we find a linear dependence of this stress on the bias field for our model as well. Note that the depolarizations stress $\sigma = -\sigma_{\mathrm{c}} = -66.6$ MPa corresponds to the

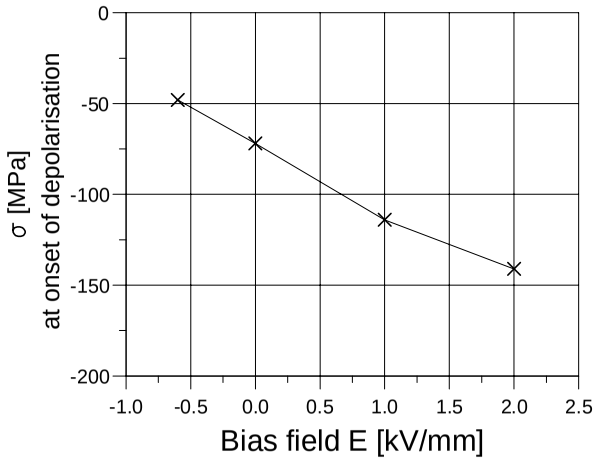

Fig. 14: Stress σ at the onset of depolarization for different values of a bias electric field E.

case of a zero bias field.

4.4 Electric cycling under bias mechanical compression

We now consider electric cycling under a compressive bias stress acting in the direction of the field. Such a bias stress gives rise to an external constraint for domain switching: The tendency of the electric field to align the c axes of the unit cells with its own direction is counteracted by the compressive stress. For sufficiently large stresses, electrically initiated switching may even be surpressed completely. For interesting experimental investigations on this matter see [27].

In order to investigate the reponse of our model for this situation, we consider the following loading history: After applying a compressive stress of -40 MPa at zero field, the electric field is cycled at an amplitude of ± 3.0 kV/mm with the stress still acting. The material parameters are the same as before. The corresponding curves are shown in Fig. 15. Compared to Figs. 5a) and 6, these hystereses look qualitatively different.

From Fig. 15a) we see that the first poling is initiated before the coercive field has been reached. Due to the presence of a mechanical stress in f_β, it takes a smaller field strength for $\sqrt{f_\beta^2 + f_\gamma^2}$ to attain its critical value. It is the total energy of the external loads that has to overcome a threshold in order to initiate irreversible processes. During poling, we do not reach a fully poled state even for E = 3.0 kV/mm. Consequently, we find a remanent polarization of only 200 mC/m^2 after unloading. Furthermore, the second step of poling attributed to 90° switching has gained significantly in size and it takes much higher field magnitudes to initiate this step of poling. In fact, the field strength of 2.0 kV/mm considered in the previous sections would not have been sufficient to induce any 90° switching at all.

a) b)

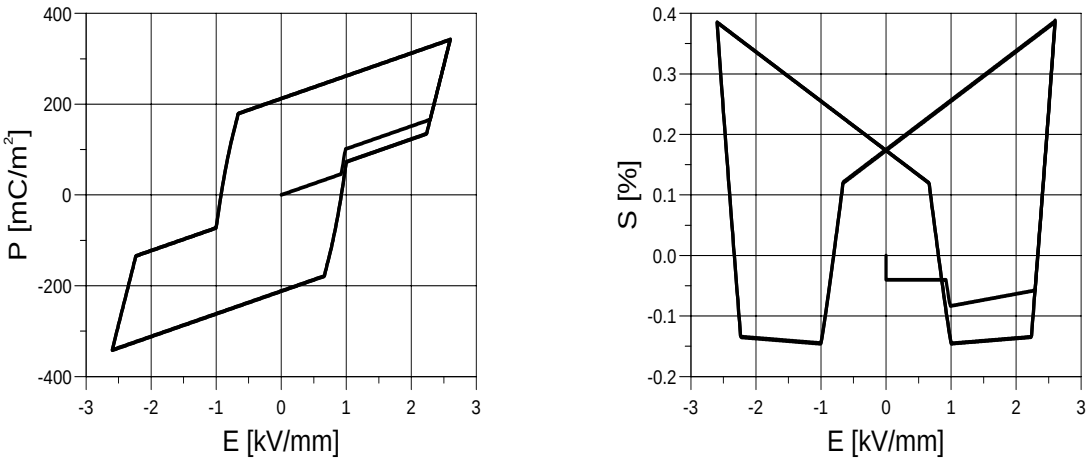

Fig. 15: Electric cycling under a compressive bias stress:
a) Dielectric hysteresis b) Butterfly hysteresis

The impact of the bias stress on the butterfly hysteresis is even more significant. First, the application of the bias stress gives rise to a linear elastic predeformation of -0.04%. Next, as the evolution of irreversible processes is initiated, we observe a small drop of the strain until the irreversible changing is paused again. As the energy level for switching is overcome, we do have a slight increase in γ, i e., some 180° switching, causing an increase of the polarization observed in Fig. 15a). But at the same time, the compressive stress in the driving force f_β leads to a reduction of β and thus to the observed corresponding drop of the irreversible strain. This can be asociated to 90° switching giving way for the bias stress. During the pause of the evolution of the internal variables, we see a linear piezoelectric changing of the strain. The slight positive slope of this part of the curve confirms that a certain degree of net polaristion already exists at this stage.

At the end of the pause, the electric field is strong enough to lead to 90° switching against the bias stress and poling as well as irreversible deformation are observed. However, as mentioned before, a fully poled state can not be reached and thus the remanent strain after unloading is considerably smaller then the saturation strain S_{sat}.

During reversing the field, the strain drops significantly below zero, indicating values of β close to zero. This may be interpreted that most of the domains assume a 90° intermediate state to give way for the bias stress before the reversed field has become strong enough to align them again with the poling axis. In the pause before the repoling starts, we observe a small slope of the E-S curve. From this piezoelectric behavior we conclude that a weak net polarization in the new direction of the electric field is already present.

In concluding this section we mention that according to further example calculations our model yields for bias stresses of sufficient strength a total suppression of any poling.

a) b)

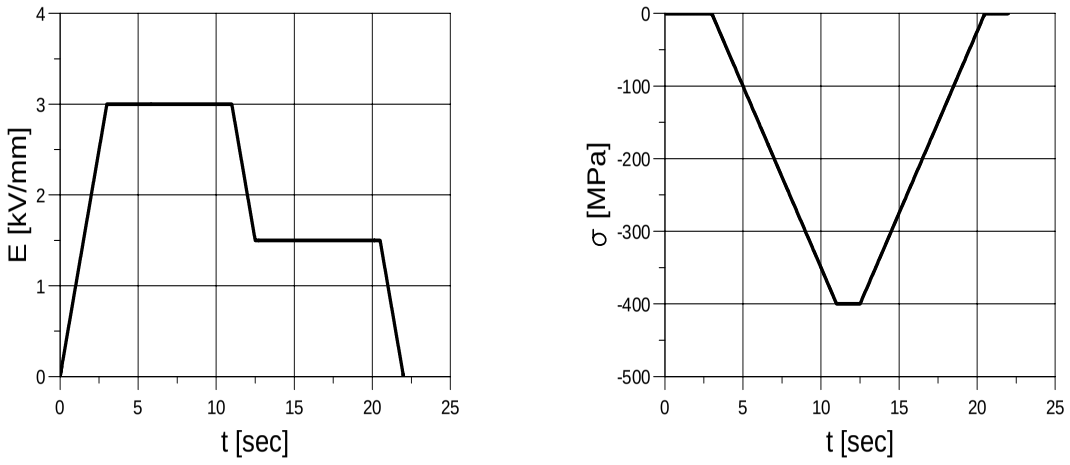

Fig. 16: Section 4.5: Electro-mechanical loading history:
a) Electric field E vs. time t
b) stress σ vs. time t

4.5 Discussion of a more complex electro-mechanical loading path

It might be interesting to validate the physical significance of our model for a more complicated non-standard loading history. In this sense, we now discuss the model response to loading history in Fig. 16. It is divided in five steps. The electric field is raised to $3\,\mathrm{E_c}$ in the first step ending at $t = 3$ sec and kept constant in the second step, during which a strong compressive stress is applied. At $t = 11$ sec a stress of -400 MPa is reached. In the third step lasting until $t = 12.5$ sec, the mechanical stress is constant and the electric field is reduced to $1.5\,\mathrm{E_c}$. It remains at this value in the fourth step, while the mechanical stress is completely removed. Finally, from $t = 20.5$ sec to $t = 22$ sec, the electric field is reduced to zero in the fifth step. The material constants were chosen as before.

In the first step ending at E = 3.0 kV/mm, we observe a poling process, see Fig. 17a), i. e., a rapid increase of the polarization once the coercive field is overcome, until the remanent polarization reaches its saturation value and further polarization changes are reversible. The reversible and irrersible straining associated to the poling process can be seen in Fig. 17b). These parts of the curves are already known from the previous sections.

In the second step, mechanical depolarization takes place. From Fig. 18b), we see that the polarization is reduced under the action of a strong compressive load. First, we observe linear piezoelectric changing but for stresses close to -180 MPa, a rapid decrease of the polarization starts. As we have seen before, such a depolarization process due to 90° switching is represented by β and γ being reduced to zero. For stesses below -190 MPa, a completely depolarized state is reached and from Fig. 17a) we see that the remaining

a) b)

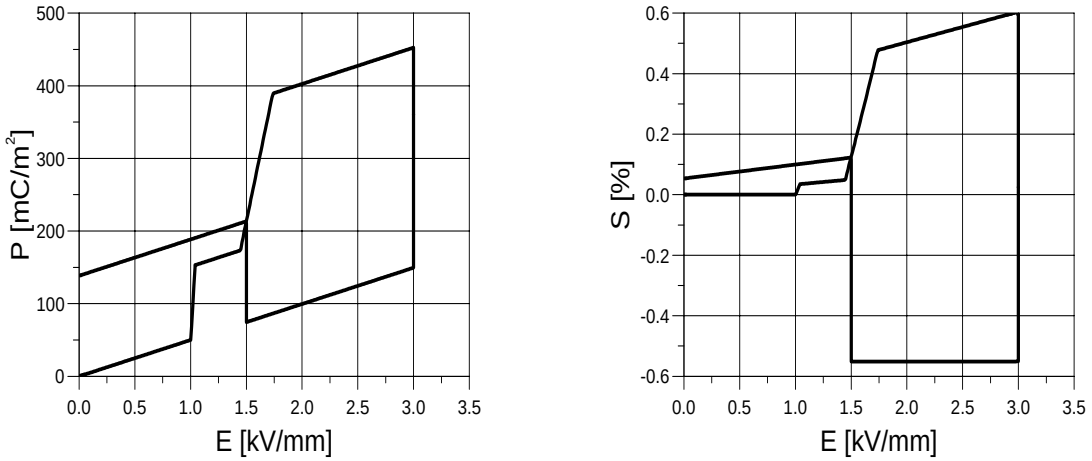

Fig. 17: Section 4.5: Model response:
a) Polarization P vs. electric field E
b) Strain S vs. electric field E

a) b)

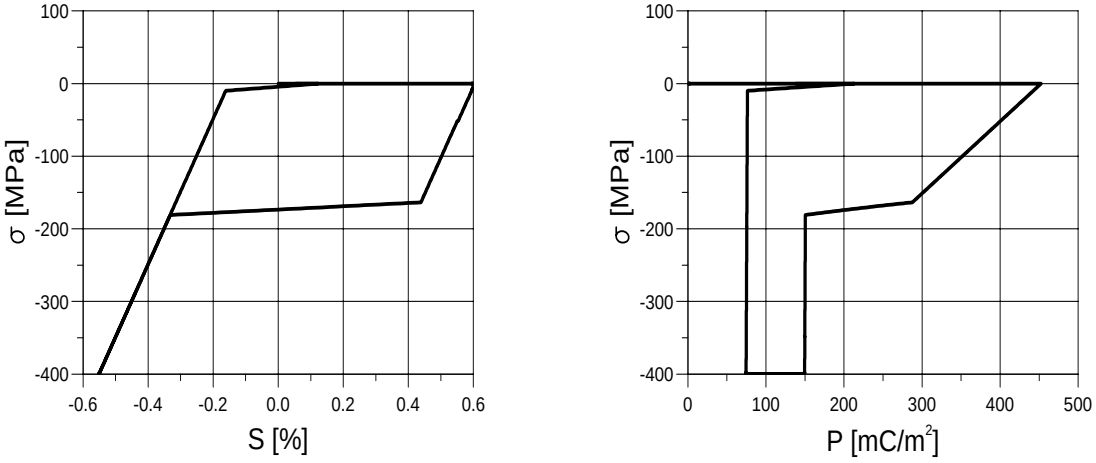

Fig. 18: Section 4.5: Model response:
a) Stress σ vs. Strain S
b) Polarization P vs. Stress σ

polarization is merely the linear dielectric contribution associated to the electric field by the dielectric constant ϵ. For compressive stress in this range there are no further changes in polarization, thereby confirming the loss of piezoelectricity and thus of net polarization. Fig. 18a) shows the deformation accompanying the depolarization. For stesses below -190 MPa, the completely depolarized state exhibits a linear elastic behavior.

The third step of reduction of the electric field leads to a linear dielectric reduction of the polarization, see Figs. 17a) and 18a). In Fig. 17b), we see that the strain is constant during the reduction of the electric field, indicating once more the absence of piezoelectric coupling.

In the fourth step, the mechanical stress is removed until $t = 20.5$ sec. However, the electric field is still above the coercive field. Because of this, repoling takes place as the compressive stress is released, and thus the microstructural parameters β and γ recover. Consequently, the polarization grows again just until it reaches the corresponding value of the first polarization curve in Fig. 17a). Furthermore, we have an associated recovery of the irreversible strain, see Fig. 18b).

Finally, upon removing in step five the electric field, the polarization and the strain are reduced to their current remanent values. From the non-zero slope of the strain over the electric field in this period observed in Fig. 17b), we conclude a limited recovery of the piezoelectricity due to the recovery of the net irreversible polarization.

5 Discussion of a more realistic formulation of the model

The model formulation discussed up to now was based on an idealised enforcement of the range of admissible values for the internal variables. In particular, this formluation leads to a step like representation of the transition from 180° to 90° switching with an intermediate pause of the evolution of the internal variables. However, in a polycrystalline ceramic we rather expect a continous transition from a behavior dominated by 180° switching to a behavior dominated by 90° switching. This transition takes place at different instants of the loading history in different grains and domains rather then at one instant everywhere in the ceramic. Beyond a certain level of the load, the number of domains undergoing the transition will gradually increase, reach a maximum, and finally die out as the transition processes are complete.

The description of the transition from 180° to 90° switching depends on the choice of the function I_G. Taking I_G to be the indicator function of the set G of admissible values for the microstructural parameters could be interpreted as surrounding this set with infinitely steep and infinetely high energy barriers. This meant that even for states (β, γ) very close to the boundary ∂G, no information about the being near transition of the switching types was available in advance.

A more realistic description of the transition from 180° to 90° switching can be achieved by modifying the choice of the funcions h_i. In this sense, we now define

$$h_1(\beta, \gamma) \;=\; (\gamma - \beta)^{-(2n+1)} \tag{70}$$

$$h_2(\beta,\gamma) \;=\; (-\gamma-\beta)^{-(2n+1)} \tag{71}$$

$$h_3(\beta,\gamma) \;=\; (\beta-1)^{-(2n+1)} \tag{72}$$

where n is a non-negative integer. The interior of the set G is then represented by

$$G\backslash\partial G = \Big\{\ (\beta,\gamma)\ \Big|\ 0 < h_i(\beta,\gamma) < \infty\ ,\ i=1,2,3\Big\} \quad . \tag{73}$$

The function I_G may then be defined as

$$I_G(\beta,\gamma) = \alpha_1 h_1 + \alpha_2 h_2 + \alpha_3 h_3 \quad , \tag{74}$$

where $\alpha_i \geq 0$ are material constants. This choice of I_G can be considered to surround G with infintite high energy barriers, but they have a finite and increasingly larger slope as ∂G is approached from the interior of G. The steepness of this walls is controlled by n.

According to the prescriptions (38) and (39), we now find

$$f_\beta = \tfrac{3}{2}\, S_{\rm sat}\, \sigma - c_\beta\, (\beta - \tfrac{1}{3}) \;-\; \frac{\alpha_1\,(2n+1)}{(\gamma-\beta)^{(2n+2)}} \;+\; \frac{\alpha_2\,(2n+1)}{(-\gamma-\beta)^{(2n+2)}} \tag{75}$$

$$\begin{aligned} f_\gamma = {} & \mathrm{P}_{\rm sat}\,\mathrm{E} + \mathrm{d}_{\rm sat}\,\sigma\,\mathrm{E} - c_\gamma\,\gamma \\ & + \frac{\alpha_1\,(2n+1)}{(\gamma-\beta)^{(2n+2)}} \;+\; \frac{\alpha_2\,(2n+1)}{(-\gamma-\beta)^{(2n+2)}} \;-\; \frac{\alpha_3\,(2n+1)}{(\beta-1)^{(2n+2)}} \end{aligned} \tag{76}$$

for the driving forces. In contrast to the previous formulation, the correction terms due to I_G are now always present. They induce an increasing counter force as the boundary ∂G is approached from the interior of I_G. The influence of these counter forces is balanced by α_i. In this sense, we now may say that the state is provided with the information about the closeness to the boundary ∂G.

5.1 Representation of the hystereses

In this section, we will have a look at the hystereses resulting from the modified model. We adopted the values of Tab. 1 for the material paramters together with $c_\beta = 100$ kPa and $c_\gamma = 50$ mC/m^2 $\cdot$ kV/mm. In order to check the basic properties of our model, we realized a rate-independent model response by $\Lambda_0 = 2.0 \cdot 10^{-3}$ sec^{-1}$\cdot$kPa^{-2}. In I_G, we took $n = 1$, $\alpha_3 = 0.1$, and $\alpha_1 = \alpha_2 = \alpha_3 2^{-(2n+2)}$.

We start with electric cycling at an amplitude of 2.0 vK/mm. The dielectric hysteresis in Fig. 19a) now has a much more realistic appearance. Since the saturation states at the boundary of G can be reached only asymptotically, we observe the typically curved transition into saturated behavior known from experiments.

In Fig. 19b) we observe a first period that may be associated to pure 180° switching. However, as the state (β,γ) approaches the boundary ∂G, the corrective contribution to (f_β, f_γ) originating from h_1 in I_G gaines influence deflecting the path of (β,γ) such that it runs parallel to ∂G. As before, this part of the model response can be associated to 90° switching processes. As the state now approaches values with $\beta = 1$, the corrective

a) b)

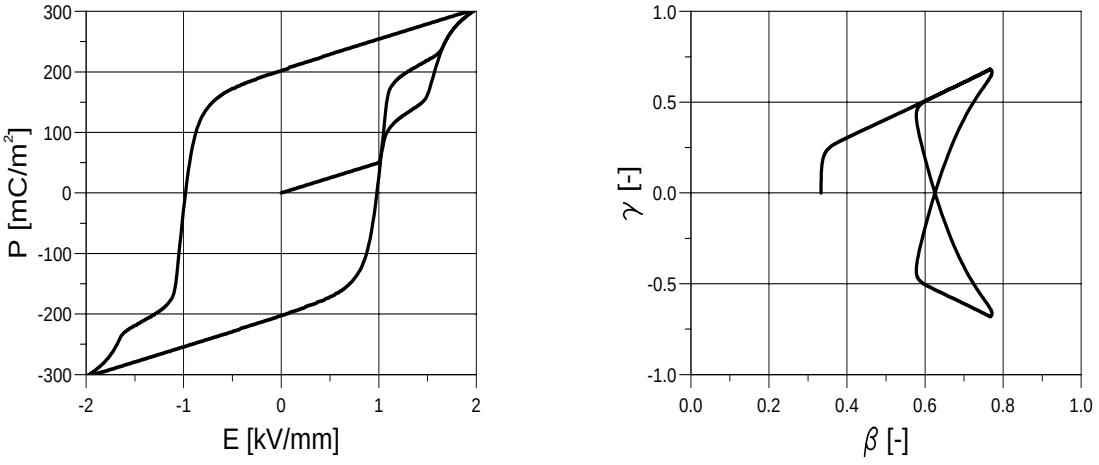

Fig. 19: Model response for the modified choice of I_G:
a) dielectric hysteresis
b) β-γ plane

contribution to (f_β, f_γ) caused by h_3 in I_G becomes inportant too, and eventually these corrective terms cancel out the external loads stopping gradulally the evolution of the internal variables near the upper right corner of G. In its microstructural interpretation, this is a state of saturated polarization where the domain structure has assumed the orientation of the acting electric field as far as possible.

A close look at Fig. 19b) reveals that (β, γ) never reaches the boundary of G. As a consequence, the remanent polarization is significantly below the saturation polarization $\mathrm{P_{sat}}$. The principal behavior of the modified model is basically the same as the before. In particular, we still can identify in the dielectric curve the periods dominated by 180° and 90° switching.

Fig. 20a) shows the corresponding butterfly hysteresis. We recognize a clearly more realistic representation of the saturation process of poling as the curve of the strain over the electric field enters gradually into the linear piezoelectric range. Obviously, this curve can be understood in view of the discussion above and in section 4.1. Similar remarks apply also to the ferroelastic hysteresis shown Fig. 20b).

6 Conclusion

The constitutive model for piezoceramics discussed in the previous sections has been contstructed on a thermodynamical basis. In order to describe the significant history dependence these materials show, we introduced microscopically motivated internal variables with ordinary differential equations as evolution laws.

a) b)

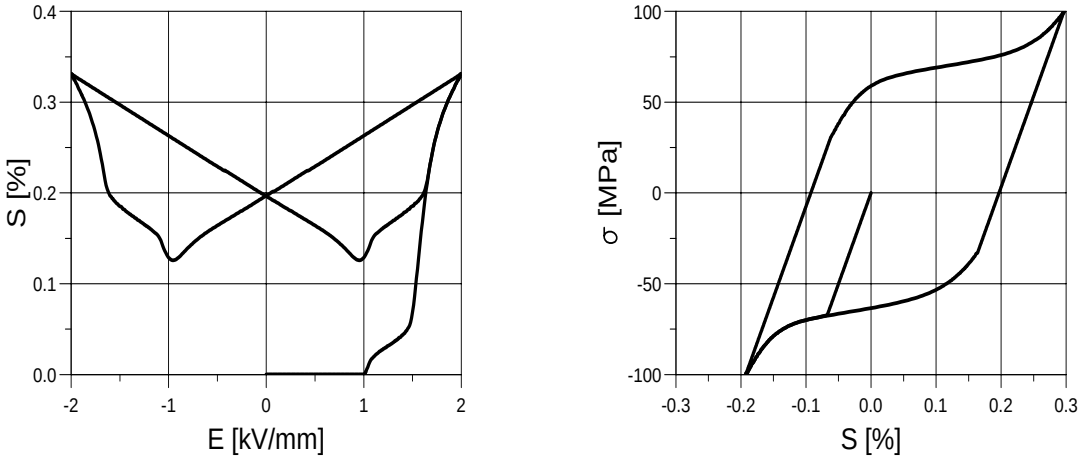

Fig. 20: Strain computation according to the modified model:
a) Butterfly hysteresis during electric cycling
b) Ferroelastic hysteresis during mechanical cycling

Even though only very few material constants are involved in the present formulation of the model, the the behavior of piezoceramics under uni-axial loadings was represented at least qualitatively well. Even more important, all observations made at the macroscopic curves of the model response could be associated to well established microscopic interpretations of ferroelectric behavior.

Further investigations concerning the shape and the enforcement of the set G of admissible values for the internal variables seem to be desirable. An improved model response can be expected, if more realistic functions for the dependence of the classical piezoelectric constants on the microstructural parameters are chosen. Finally, the rate dependence of the model response needs to be compared more thouroughly to experimental results, possibly leading to a modification of the factor Λ in the evolution equations.

Acknowledgement–The work reported in this paper has been carried out during a stay of Q. J. at FZK, June 19 through September 14, 1997, and a stay of M. K. at UCR, April 1 through June 30, 1998. The authors thank Prof. D. Munz for his encouragement and support. Q. J. thanks DAAD for financial support of his visit at FZK. Support by the Deutsche Forschungsgemeinschaft, Bonn, and by the U. S. Office of Naval Research is gratefully acknowledged.

References

[1] Kumar, S.; Bhalla, A. S.; Cross, L. E.: Smart Ferroelectrics for Acoustic and Vibration Control, J Intell Mater Syst Struct **5**(1994), 678 - 682

[2] Newnham, R. E.: Electroceramics, Rep Prog Phys **52**(1989), 123 - 156

[3] Cross, L. E.: Ferroelectric ceramics: Tailoring Properties for specific applications, Ferroelectric ceramics: tutorial reviews, theory, processing, and applications (Eds.: N. Setter and E. L. Colla) (Birkhäuser Verlag) Basel 1993, 1 - 86

[4] Cross, L. E.: Ferroelectric Materials for Electromechanical Transducer Applications, Jpn J Appl Phys **34**(1995), 2525 - 2532

[5] Li, S.; Cao, W.; Cross, L. E.: The extrinsic Nature of nonlinear behavior Observed in Lead Zirconate Titanate Ferroelectric Ceramic, J Appl Phys **69**(1991), 7219 - 7224

[6] Jiang, Q. Y.; Cross, L. E.: Effect of Porosity on Electric Fatigue Behavior in PLZT and PZT Ceramics, J Mater Sci **28**(1993), 4536 - 4543

[7] Jiang, Q. Y.; Cao, W.; Cross, L. E.: Electric Fatigue in Lead Zirconate Titanate Ceramics, J Am Ceram Soc **77**(1994), 211 - 215

[8] Maugin, G. A.: Continuum Mechanics of Electromagnetic Solids, (Elsevier Science Publishers) Amsterdam *et al.* 1988

[9] Parton, V. Z.; Kudryavtsev, B. A.: Electromagnetoelasticity. Piezoelectrics and Electrically Conductive Solids, (Gordon and Breach Science Publishers) New York *et al.* 1988

[10] Gaudenzi, P.; Bathe K.-J.: An Iterative Finite Element Procedure for the Analysis of Piezoelectric Continua, J Intelligent Material Systems Structures, **6**(1995), 266 - 273

[11] McMeeking, R. M.: Electrostrictive Stresses Near Crack-Like Flaws, ZAMP, **40**(1989), 615 - 627

[12] Pak, Y. E.: Linear electro-elastic fracture mechanics of piezoelectric materials, Int J Fracture, **54**(1992), 79 - 100

[13] Suo, Z.; Kuo, C.-M.; Barnett, D. M.; Willis, J. R.: Fracture Mechanics for Piezoelectric Ceramics, J Mech Phys Solids, **40**(1992), 739 - 765

[14] Sosa, H.: On the Fracture Mechanics od Piezoelectric Solids, Int J Solids Structures **29**(1992), 2613 - 2622

[15] Dunn, M.: The Effect of Crack Face Boundary Conditions on the Fracture Mechanics of Piezoelectric Solids, Engng Fract Mech, **48**(1994), 25 - 39

[16] Kumar, S.; Singh, R. N.: Crack Propagtion in Piezoelectric Materials under Combined Mechanical and Electrical Loadings, Acta Mater, **44**(1996), 173 - 200

[17] Govorukha, V. B.; Munz, D.; Kamlah, M.: Investigation of a Bimaterial Piezoelectric Plane with an Interface Crack, ZAMM **78**(1998)

[18] Chen, P. J.; Tucker, T. J.: Determination of the Polar Equilibrium Properties of the Ferroelectric Ceramic PZT 65/35, Acta Mech, **38**(1981), 209 - 218

[19] Chen, P. J.; Peercy, P. S.: One Dimensional Dynamic Electromechanical Constitutive Relations of Ferroelectric Materials, Acta Mech, **31**(1979), 231 - 241

[20] Chen, P. J.; Marsden M. M.: One Dimensional Polar Responses of the Electrooptic Ceramic PLZT 7/65/35 Due to Domain Switching, Acta Mech, **41**(1981), 255 - 264

[21] Chen, P. J.: Three Dimensional Dynamic Electromechanical Constitutive Relations for Ferroelectric Materials, Int J Solids Structures, **16**(1980), 1059 - 1067

[22] Chen, P. J.: Hysteresis Effects in Deformable Ceramics, The Mechanical Behavior of Electromagnetic Solid Continua (Ed. G. A. Maugin), (Elsevier Science Publishers) IUTAM 1984, 137 - 143

[23] Bassiouny, E.; Ghaleb, A. F.; Maugin, G. A.: Thermomechanical Formulation for Coupled Electromechanical Hysteresis Effects–I. Basic Equations, II. Poling of Ceramics, Int J Engng Sci, **26**(1988), 1279 - 1306

[24] Bassiouny, E.; Maugin, G. A.: Thermomechanical Formulation for Coupled Electromechanical Hysteresis Effects–III. Parameter Identification, IV. Combined Electromechanical Loading, Int J Engng Sci, **27**(1989), 975 - 1000

[25] Cao, H.; Evans, A. G.: Nonlinear Deformation of Ferroelectric Ceramics, J Am Ceram Soc, **76**(1993), 890 - 896

[26] Schäufele, A.; Härdtl, K. H.: Ferroelastic Properties of Lead Zirconate Titanate Ceramics, J Am Soc **79**(1996), 2637 - 2640

[27] Lynch, C. S.: The Effect of Uniaxial Stress on the Electro-Mechanical Response of 8/65/35 PLZT Acta Mater, **44**(1996), 4137 - 4148

[28] Suo, Z.: Mechanics Concepts for Failure in Ferroelectric Ceramics, Smart Structures and Materials (Ed. A. V. Srinivasan), AD-Vol. 24, AMD-Vol. 123, (ASME) New York 1991, 1 - 6

[29] Hom, C. L.; Shankar, N.: A Fully Coupled Constitutive Model for Electrostrictive Ceramic Materials, J Intelligent Material Systems Structures, **5**(1994), 795 - 801

[30] Yang, W.; Suo, Z.: Cracking in Ceramic Actuators Caused by Electrostriction, J Mech Phys Solids, **42**(1994), 649 - 663

[31] Hao, T. H.; Gong, X.; Suo, Z.: Fracture Mechanics for the Design of Ceramic Multilayer Actuators, J Mech Phys Solids, **44**(1996), 23 - 48

[32] Kamlah, M.; Tsakmakis. C.: Phenomenological Modeling of the Non-Linear Electro-Mechanical Coupling in Ferroelectrics, In press, Int. J. Solids Structures

[33] Hwang, S. C.; Lynch, C. S.; McMeeking, R. M.: Ferroelectric/Ferroelastic Interactions and a Polarization Switching Model, Acta Metall Mater **43**(1995), 2073 - 2084

[34] Michelitsch, T.; Kreher, W.: A Simple Model for the Nonlinear Material Behavior of Ferroelctrics, Acta Mater. **46**(1998), 5085 - 5094

[35] Kim, S. J.; Jiang, Q.: Microcracking and electric fatigue of polycrystalline ferroelectric ceramics, Smart Mater Struct **5**(1997), 321 - 326

[36] Huo, Y.; Jiang, Q.: Modeling of Domain Switching in Polycrystalline Ferroelektric Ceramics, Smart Mater Struct **6**(1997), 441 - 447

[37] Huo, Y.; Jiang, Q.: Modeling of Domain Switching in Ferroelektric Ceramics: An Example, Int J Solids Structures **35**(1998), 1339 - 1353

[38] Wang, Y.: Numerical Simulation on Fatigue Behavior of Ferroelectric Ceramics. Dissertation thesis, University of Nebraska, Lincoln 1997

[39] Jaffe, B.; Cook, W. R.; Jaffe, H.: Piezoelectric Ceramics, (Academic Press) London New York 1971

[40] Fett, T,.; Munz, D.; Thun, G.: Nonsymmetric Deformation Behavior of Lead Zirconate Titanate Determined in Bending Tests, J Am Ceram Soc **81**(1998), 269 - 272

[41] Frémond, M.: Internal Constraints and Constitutive Laws, Mathematical Models for Phase Change Problems (Ed. J. F. Rodrigues). International Series of Numerical Mathematics. Vol. 88. Basel 1989, 3 - 18

[42] Savi, M.; Braga, A.; Alves, J.; Almeida, C.: Finite Element Model for Trusses with Shape Memory Alloy Actuators, Proceedings of the Euromech 373 Colloquium "Modelling and Control of Adaptive Mechanical Structures", Otto-von-Guericke Universität, Magdeburg 1998, (Ed. U. Gabbert). Fortschritt-Berichte VDI, Vol. 11/268, 115 - 124